



# Constitutive modelling of hydrolytic degradation in hydrogels

Zhouzhou Pan, Laurence Brassart \*

Department of Engineering Science, University of Oxford, Oxford OX1 3PJ, United Kingdom

## ARTICLE INFO

### Keywords:

Polymers  
Hydrolysis  
Swelling  
Rubber elasticity  
Multiphysics couplings

## ABSTRACT

Biodegradable synthetic hydrogels have emerged as promising materials for tissue engineering and drug/cell delivery applications. However, their successful implementation requires precise understanding of the degradation response in terms of mechanical properties, swelling, and mass loss. In this work, we develop a thermodynamically-consistent continuum framework and constitutive models for coupled large deformation and hydrolytic degradation in hydrogels. In particular, we propose constitutive models for the evolution of elastic modulus and polymer mass loss based on a description of the evolving network topology during hydrolysis. The theory is validated against experimental data for two model hydrogel systems with different network architectures, namely biodegradable Tetra-PEG hydrogels and PLA-b-PEG-b-PLA hydrogels. We have also implemented our model in a finite element software. We show that our model is capable of simulating degradation-induced heterogeneous swelling in scenarios relevant to biomedical applications. Our theory and constitutive models could be useful for the design of hydrogels with controlled degradation behaviour.

## 1. Introduction

Hydrogels consist of hydrophilic polymer networks swollen by a large amount of water. Key properties of hydrogels include low modulus, high deformability and ability to respond to a variety of environmental cues, making them suitable for a broad range of biomedical applications. For example, hydrogels are used for the controlled release of drugs via their stimuli-responsive swelling response (Park et al., 1993; Liu et al., 2015; Li and Mooney, 2016; Fu et al., 2018; Rizzo and Kehr, 2021). They are also developed as scaffolds for tissue engineering, providing an environment conducive for cell growth (Slaughter et al., 2009; Xue et al., 2021). In these applications, it is important to control the degradation behaviour of hydrogels over time, for example to induce drug release via degradation-induced swelling, or to synchronise scaffold degradation with natural tissue growth (Kamata et al., 2015; Bryant and Vernerey, 2018).

This paper focuses on hydrolytic degradation, which is a common degradation mechanism in many hydrogels. During hydrolysis, water molecules react with ester, amide or ether groups and cause the scission of polymer chains. Gradual chain scission in turn induces a deterioration in mechanical properties by reducing the number of elastically effective chains in the polymer network. Chain scission also produces short chains detached from the polymer network and which are being released by diffusion, leading to polymer mass loss. Both modulus reduction and polymer mass loss directly impact the swelling behaviour. In order to design biodegradable hydrogel-based devices with controlled mechanical and swelling properties over their service life, it is necessary to develop in-depth understanding of the relationships between degradation, mechanical properties and swelling.

A number of experimental studies have investigated the behaviour of hydrogels during hydrolytic degradation (Metters et al., 2000a; Zustiak and Leach, 2010; Li et al., 2011; Castilla-Cortázar et al., 2012; Diederich et al., 2017; Lueckgen et al., 2018; Shi et al.,

\* Corresponding author.

E-mail address: [laurence.brassart@eng.ox.ac.uk](mailto:laurence.brassart@eng.ox.ac.uk) (L. Brassart).

2021). For example, Metters et al. (2000a) studied the degradation behaviour of model hydrogels consisting of triblock PLA-b-PEG-b-PLA copolymers connecting long polyacrylate chains. These authors found that the elastic modulus and swelling ratio of degrading gels evolve approximately exponentially with time, and related their respective time constants using simple scaling relations (Metters et al., 2001a). In contrast, the mass loss fraction was found to evolve almost linearly with time for most of the degradation process, before sharply increasing during the final degradation stage. Diederich et al. (2017) showed that the mechanical and degradation properties of PLA-b-PEG-b-PLA hydrogels could be tailored by changing the polymer concentration and the number of hydrolysable units within the triblock copolymer crosslinks. Other studies have focused on the design of hydrogels where the mechanical and degradation properties can be controlled independently (Cha et al., 2009; Li et al., 2011). For example, Cha et al. (2009) utilised oxidised methacrylic alginate as a biodegradable crosslinker in model hydrogels. They showed that degradability can be tuned by altering the oxidation degree of the crosslinker without changing the modulus of the network. Li et al. (2011) introduced the concept of tunable degradability in near-ideal Tetra-PEG hydrogels, which are formed by the A-B type cross-end reaction of four-arm PEG macromolecules in solution (Sakai et al., 2008). The degradability could be precisely controlled by changing the relative amount of Tetra-PEG units having degradable and non-degradable end groups.

Computational models have a role to play in accelerating the development of degradable hydrogels with controlled mechanical and swelling behaviour. The continuum mechanics framework for large elastic deformations coupled to mass transport is now well-established, see e.g. Hong et al. (2008), Chester and Anand (2010), Lucantonio et al. (2013) and the reviews Liu et al. (2015), Huang et al. (2020), Lei et al. (2021b). In recent years, modelling efforts from the solid mechanics community have mainly addressed the rate-dependent and damage response of hydrogels (Drozdov, 2017; Mao et al., 2017; Wang et al., 2017; Morovati and Dargazany, 2019; Bosnjak et al., 2020; Lu et al., 2020; Lamont et al., 2021; Liu et al., 2022), to name only a few. Many of these works were motivated by the emergence of double-network gels and other model systems with exceptional mechanical properties. These models are however limited in their ability to link the evolving network structure to the mechanical properties, because they rely on a very simplified representation of the underlying network. To address this, mesoscopic models have also emerged in recent years (Kothari et al., 2018; Alamé and Brassart, 2019, 2020; Lei et al., 2021a; Wagner et al., 2022).

In contrast, there have been limited attempts so far at modelling the coupled degradation and deformation response of hydrogels. Notably, Li et al. (2011) modified the Flory–Rehner equation to account for the evolving modulus to describe degradation-induced swelling in Tetra-PEG hydrogels. These authors used the Phantom model combined with tree-like theory to express the modulus as a function of network connectivity down to the point of reverse gelation (the point at which the gel loses all its integrity). However, their model neglected mass loss. Dhote and Vernerey (2014) developed a thermodynamic model for coupled degradation, swelling, and transport of solute molecules (here, extracellular matrix molecules) released during degradation. However, the degradation model did not rely on a description of the underlying degrading network and also neglected polymer mass loss. Zhou and Jin (2020) proposed a model for the hydrolysis-induced swelling of polyelectrolyte gels. Their model described the change of polyacrylamide hydrogel from a neutral hydrogel to a polyelectrolyte hydrogel due to the hydrolytic reaction, and its effect on osmotic pressure (and therefore swelling). Their model also accounted for auto-retarding kinetics. However, the effect of degradation on the network elasticity was not taken into account. Other studies adopted a statistical approach to describe mass loss during degradation. The effect of degradation on the modulus was either overlooked (Metters et al., 2000b, 2001b) or expressed in terms of the crosslink density using the classical affine model of rubber elasticity (Gilormini et al., 2014; Diederich et al., 2017). We also note that constitutive models for the concurrent deformation and degradation of polymers subjected to environmental conditions have also been developed lately, e.g. Konica and Sain (2020), Bahrololoumi et al. (2020), Konica and Sain (2021), Bahrololoumi et al. (2021a,b), Najmeddine et al. (2022).

The objective of this work is to propose a general thermodynamically-consistent constitutive framework for biodegradable hydrogels coupling chemical degradation and large deformations. To this end, we build on the framework for coupled deformation and diffusion initially proposed for non-degradable hydrogels (Hong et al., 2008; Chester and Anand, 2010) and extend it to account for chemical reaction-induced damage. Since the timescale for chemical degradation is considerably longer than the timescale for diffusion, we develop the theory under the assumption of fast diffusion of water molecules and reaction products. Specific constitutive models are proposed to describe the effect of degradation on elastic modulus and mass loss in two model polymer systems: PEG-b-PLA hydrogels and Tetra-PEG hydrogels. The theory is validated against experimental data (Metters et al., 2000a; Diederich et al., 2017; Li et al., 2011). We have implemented our theory in the finite element software Abaqus through user sub-routines, and the model capability is illustrated in numerical examples of inhomogeneous swelling induced by degradation.

The paper is organised as follows. Section 2 describes hydrolytic degradation in hydrogels and introduces relevant state variables. In Section 3, we present the thermodynamic framework for coupled degradation, large deformation, and mass transport in the limit of fast diffusion. Section 4 introduces specific forms of the free energy function and kinetic models. In Sections 5 and 6, we develop material-specific expressions for the elastic modulus and mass loss in terms of the evolving network parameters for Tetra-PEG hydrogels and PEG-b-PLA hydrogels, and compare model predictions to experimental data for free swelling. Section 7 further illustrates the model capability in simple cases of homogeneous deformation under stress. In Section 8, we explore scenarios of inhomogeneous swelling induced by degradation, before concluding.

## 2. Hydrolytic degradation

We consider networks of long polymer chains that contain bonds that can be broken by chemical reaction with water. To fix the ideas, we assume that the polymer chains contain ester bonds. The hydrolysis reaction can then be written as Pan (2014):



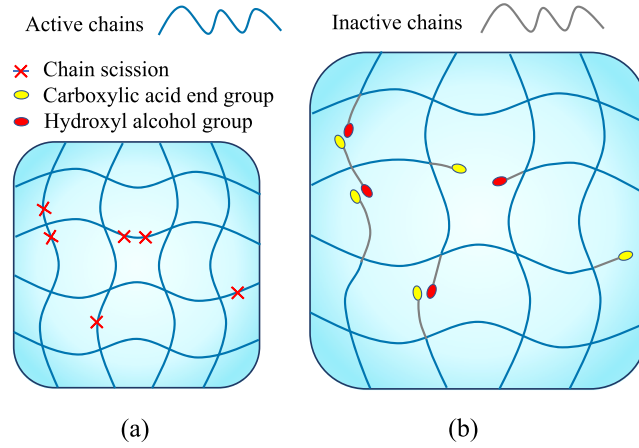


Fig. 1. Schematic representation of hydrolytic degradation in a hydrogel: (a) undegraded state and (b) degraded state. Inactive chains do not contribute to the elasticity of the network.

where  $RCOOR'$  represents a polymer strand containing an ester bond,  $R$  and  $R'$  are the remainders of the polymer chain,  $H_2O$  is the water molecule, and  $COOH$  and  $OH$  respectively represent the carboxylic acid and hydroxyl alcohol end groups. The chain scission process in a swollen polymer network is illustrated in Fig. 1. We describe the degradation state through the extent of hydrolysis reaction  $\zeta \in [0, 1]$ , defined as:

$$\zeta(\mathbf{x}, t) := 1 - \frac{[e]}{[e]_0} \quad (2)$$

where  $[e]_0$  and  $[e]$  represent the initial and current concentrations of ester bonds (number of ester bonds per unit reference volume).  $\zeta = 0$  represents the undegraded state, and  $\zeta = 1$  represents the fully degraded state where all esters bonds have reacted. In general, the extent of reaction is a function of (macroscopic) position  $\mathbf{x}$  and time  $t$ .

Hydrolysis-induced chain scission produces elastically-ineffective dangling chains and disconnected short chains, thereby reducing the elastic modulus of the hydrogel. We write  $G = G(\zeta)$  the elastic shear modulus of the dry network, a decreasing function of  $\zeta$ . We note from the outset that a hydrogel will lose all its mechanical integrity (i.e.  $G = 0$ ) at a threshold value  $\zeta_c \leq 1$  (reverse gelation point), which corresponds to the network percolation threshold. This transition may take place well before all ester bonds have degraded. As reaction proceeds, chains disconnected from the polymer network dissolve and migrate out of the hydrogel by diffusion, leading to polymer mass loss. We write  $f = f(\zeta)$  the mass loss fraction relative to the initial (dry) polymer mass. The functions  $G(\zeta)$  and  $f(\zeta)$  in general depend on the network topology. Specific models for  $G(\zeta)$  and  $f(\zeta)$  will be proposed in Sections 5 and 6 for two different classes of hydrogels.

In this work we focus on the hydrogel deformation response over the degradation timescale. Over this timescale, we may assume that diffusion of water and short chains instantaneously relaxes and reaches a pseudo steady state for the current degradation stage. We further assume that the pseudo steady state concentration of short chains is negligible, and consequently we do not list the concentration of short chains as a variable. Let  $C$  be the nominal concentration of water (number of water molecules per unit volume of dry, undegraded polymer). Neglecting the volume fraction of the short chains, the current polymer volume fraction in the degraded, swollen gel,  $\phi$  is related to the water nominal concentration and mass loss fraction by:

$$\phi = \left(1 + \frac{vC}{1-f}\right)^{-1} = (1 + v\tilde{C})^{-1} \quad (3)$$

where  $v$  is the volume per water molecule and  $\tilde{C} := C/(1-f)$  is the concentration of water measured per unit volume in the dry degraded network. The polymer volume fraction is the reciprocal of the volumetric swelling ratio  $Q$ , defined as the ratio of swollen polymer volume to the dry polymer volume at the same degradation stage (i.e. at constant  $\zeta$ ):

$$Q = \frac{1}{\phi} \quad (4)$$

Note that this definition of volumetric swelling ratio measures the change of volume due to the absorption of water with respect to the dry *degraded* network.

The central question of this study is to understand and predict the evolution of elastic modulus, mass loss and swelling ratio (three quantities frequently reported in experimental studies) over degradation time scales.

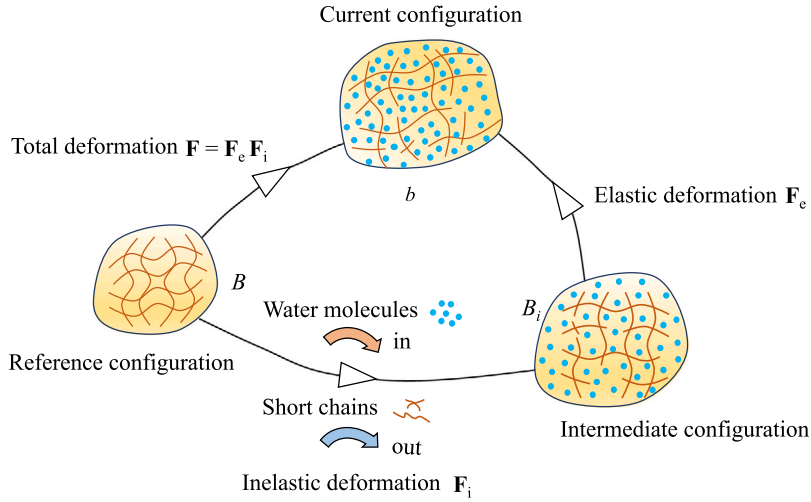


Fig. 2. Multiplicative decomposition of the deformation gradient into inelastic and elastic parts. The inelastic deformation is associated with the absorption of water and release of short polymer chains. The elastic part is associated with the distortion of the polymer network.

### 3. Continuum thermodynamic framework

#### 3.1. Kinematics

To describe hydrolysis under external loads in a hydrogel with arbitrary geometry, we adopt a large deformation continuum mechanics framework and take the dry, undegraded state as the reference state. In the current state, the hydrogel deforms under the combined actions of external forces, absorption of water and chemical degradation. Let  $\mathbf{X}$  denote the position of a material point in the reference state. In the current state, the position of the material point is described by the one-to-one mapping  $\mathbf{x} = \mathbf{x}(\mathbf{X}, t)$ , and the material velocity is  $\mathbf{v} = \dot{\mathbf{x}}$ . The relative motion of material points is measured through the deformation gradient:

$$\mathbf{F} = \frac{\partial \mathbf{x}}{\partial \mathbf{X}} \quad (5)$$

We also introduce the Jacobian:  $J = \det(\mathbf{F}) > 0$ .

We regard the local deformation as the succession of two distinct mechanisms: (1) the inelastic volume change induced by changing composition (by absorbing water molecules and by releasing short polymer chains), and (2) the elastic distortion of the remaining polymer network. Accordingly, we adopt a multiplicative decomposition of the deformation gradient:

$$\mathbf{F} = \mathbf{F}^e \mathbf{F}^i \quad (6)$$

where  $\mathbf{F}^e$  and  $\mathbf{F}^i$  represent the elastic and inelastic contributions to the deformation gradient, respectively. We also define  $J^e = \det(\mathbf{F}^e) > 0$  and  $J^i = \det(\mathbf{F}^i) > 0$ , such that  $J = J^e J^i$ . The multiplicative decomposition of  $\mathbf{F}$  is illustrated in Fig. 2

The inelastic part of the deformation gradient is taken of the following isotropic form:

$$\mathbf{F}^i = \lambda^i \mathbf{1} = (J^i)^{1/3} \mathbf{1} \quad (7)$$

where  $\lambda^i$  is the inelastic stretch. Following previous theories for hydrogels (Hong et al., 2008; Chester and Anand, 2010), we treat the polymer and solvent molecules as incompressible, and also neglect the volume change due to mixing. Therefore, the volume of the mixture of polymer and water is given by the sum of the volumes of the constituents. Incompressibility of the polymer also means that the mass fraction  $f$  is identical to the ratio of current polymer volume over initial polymer volume. The inelastic volume change is thus given by:

$$J^i = (1 - f) + vC = (1 - f)(1 + v\bar{C}) \quad (8)$$

In the first equality, the first term corresponds to the reduction in volume associated with degradation-induced polymer mass loss, and the second term is the change in volume due to swelling by absorbing water. The second equality suggests a further multiplicative decomposition of the inelastic stretch into a volume reduction part due to polymer mass loss, and a swelling part due to absorption of water in the degraded network:

$$\lambda^i = \lambda^s \lambda^d, \quad \lambda^s := (1 + v\bar{C})^{1/3} = \phi^{-1/3}, \quad \lambda^d := (1 - f)^{1/3} \quad (9)$$

This decomposition allows us to define the dry, degraded state, as an alternative reference state. The dry degraded state is useful to analyse experimental data for the swelling ratio reported in the literature, which are often measured with respect to the dry degraded network.

### 3.2. Balance of forces and moments

Consider a sub-part of a hydrogel body subjected to a field of surface traction  $\mathbf{T}(\mathbf{X}, t)$  (force per unit area in the reference configuration) and a field of body force  $\mathbf{B}(\mathbf{X}, t)$  (force per unit volume in the reference configuration). Neglecting inertial effects, force balance on an infinitesimally-small sub-part requires that:

$$\nabla \cdot \mathbf{P} + \mathbf{B} = \mathbf{0} \quad (10)$$

where  $\mathbf{P}$  is the first Piola–Kirchhoff stress tensor. The first Piola–Kirchhoff stress  $\mathbf{P}$  tensor and traction vector  $\mathbf{T}$  are related by Cauchy's relation:

$$\mathbf{T} = \mathbf{P} \cdot \mathbf{N} \quad (11)$$

where  $\mathbf{N}$  is the unit outward normal vector to a plane in the reference configuration. On the other end, balance of moments requires that  $\mathbf{P}\mathbf{F}^T = \mathbf{F}\mathbf{P}^T$ . We also recall the usual relations between the Cauchy stress tensor and the first Piola–Kirchhoff stress tensor:

$$\mathbf{P} = \mathbf{J}\boldsymbol{\sigma}\mathbf{F}^{-T}, \quad \boldsymbol{\sigma} = \mathbf{J}^{-1}\mathbf{P}\mathbf{F}^T \quad (12)$$

### 3.3. Conservation of mobile species

There are two types of mobile species in the degrading hydrogel: water molecules, and short polymer chains detached from the network. Given that the timescale for hydrolytic degradation is much longer than the timescale for diffusion of both species (Amsden, 1998; Wang et al., 2012; Fujiyabu et al., 2019; Zhou et al., 2022), we make the following two modelling assumptions:

- In the limit of fast diffusion, and for a hydrogel in contact with a reservoir of water, the concentration of short polymer chains is assumed to be negligible. Consequently we do not list the concentration of short polymer chains as a state variable.
- The concentration of water obeys a (pseudo) steady-state diffusion equation within the hydrogel body at all times. Water concentration is however not constant in time.

In view of subsequent thermodynamic treatment, we recall the condition of conservation of water molecules in its transient form:

$$\dot{\mathbf{C}} = -\nabla \cdot \mathbf{J} \quad (13)$$

where  $\mathbf{J}$  is the nominal water flux (number of molecules per unit time and area in the reference configuration). Here, we have assumed that the amount of water consumed by the hydrolysis reaction (cf. Eq. (1)) is negligible compared to the total amount of water in the hydrogel.

### 3.4. Free energy imbalance

Our constitutive theory rests on a free energy inequality for coupled large deformation and diffusion, as proposed in earlier works Hong et al. (2008), Chester and Anand (2010). We regard a sub-part  $P$  of degrading hydrogel as a thermodynamic system in contact with a heat bath and a reservoir of water molecules. Assuming a constant uniform temperature, thermodynamics requires that the power of the external agents be larger than the total change in free energy of the hydrogel:

$$\frac{d}{dt} \int_P \psi \, dV \leq \int_P \mathbf{B} \cdot \mathbf{v} \, dV + \int_{\partial P} \mathbf{T} \cdot \mathbf{v} \, dA - \int_{\partial P} \mu \mathbf{J} \cdot \mathbf{N} \, dA \quad (14)$$

where  $\psi$  is the free energy density of the hydrogel (energy per unit volume in the reference configuration) and  $\mu$  is the chemical potential of water in the environment. In Eq. (14), the first term on the right-hand side is the power of the body forces, the second term is the power of the external tractions, and the third term is the chemical power supplied by diffusion of water through the boundary. Chemical power supplied by diffusion of short chains through the boundary is not included, since short chains are not represented explicitly in our theory. Bringing the time derivative inside the integral, inserting Cauchy's relation (11) and using the divergence theorem, we obtain:

$$\int_P \dot{\psi} \, dV \leq \int_P (\mathbf{P} : \dot{\mathbf{F}} - \mu \nabla \cdot \mathbf{J} - \mathbf{J} \cdot \nabla \mu) \, dV + \int_{\partial P} (\nabla \cdot \mathbf{P} + \mathbf{B}) \cdot \mathbf{v} \, dV \quad (15)$$

Using the equilibrium condition (10) and the condition of conservation of water molecules (13), and requiring the inequality (15) to hold for arbitrarily small volume, we obtain the following local inequality:

$$\mathbf{P} : \dot{\mathbf{F}} + \mu \dot{\mathbf{C}} - \dot{\psi} - \mathbf{J} \cdot \text{Grad} \mu \geq 0 \quad (16)$$

Inserting the multiplicative decomposition of  $\mathbf{F}$  (6), the stress power is re-expressed as (Chester and Anand, 2010):

$$\mathbf{P} : \dot{\mathbf{F}} = \mathbf{P}^e : \dot{\mathbf{F}}^e + \mathbf{M}^i : \mathbf{L}^i \quad (17)$$

where the stress-like tensors  $\mathbf{P}^e$  and  $\mathbf{M}^i$  are defined as

$$\mathbf{P}^e := \mathbf{P}\mathbf{F}^{iT}, \quad \mathbf{M}^i := \mathbf{F}^{eT} \mathbf{P}\mathbf{F}^{iT} \quad (18)$$

and  $L^i$  is the inelastic spatial velocity gradient:

$$L^i = \dot{F}^i F^{i-1} \quad (19)$$

Using Eq. (7), the stress power (17) simplifies as:

$$P : \dot{F} = P^e : \dot{F}^e - p j^i \quad (20)$$

where

$$p := -\frac{1}{3} J^e \text{tr}(\sigma) \quad (21)$$

We assume that all the volume change arises from the change in composition (absorption of water and release of short polymer chains) and therefore take  $J^e = 1$  (and  $\dot{J}^e = 0$ ). It then follows that  $F^{e-T} : \dot{F}^e = 0$ , and that the elastic stress power can be rewritten as:

$$P^e : \dot{F}^e = P^e : \dot{F}^e + J \Pi F^{e-T} : \dot{F}^e \quad (22)$$

where  $\Pi$  is an arbitrary scalar field representing an a-priori unknown hydrostatic pressure, to be identified from the boundary conditions. Using Eqs (8), (20) and (22), the dissipation inequality (16) is rewritten as:

$$(P^e + J \Pi F^{e-T}) : \dot{F}^e + (\mu - pv)\dot{C} + p f' \dot{\zeta} - \dot{\psi} - J \cdot \nabla \mu \geq 0 \quad (23)$$

where  $f' = df/d\zeta$ .

### 3.5. State laws and reduced inequality

Our theory for coupled deformation and degradation involves three independent state variables: the elastic deformation gradient  $F^e$ , the nominal concentration of water  $C$ , and the extent of reaction  $\zeta$ . Accordingly, the free energy is taken of the following form:

$$\psi = \psi(F^e, C, \zeta) \quad (24)$$

The inequality (23) becomes:

$$\left( P^e + J \Pi F^{e-T} - \frac{\partial \psi}{\partial F^e} \right) : \dot{F}^e + \left( \mu - pv - \frac{\partial \psi}{\partial C} \right) \dot{C} + \left( p f' - \frac{\partial \psi}{\partial \zeta} \right) \dot{\zeta} - J \cdot \nabla \mu \geq 0 \quad (25)$$

We neglect viscoelasticity of the polymer network and therefore assume that the dissipation associated with elastic distortion vanishes at all times. This leads to the state law for the stress:

$$P^e = \frac{\partial \psi}{\partial F^e} - J \Pi F^{e-T} \quad (26)$$

Using Eq. (18), the first Piola–Kirchhoff stress is readily obtained:

$$P = \frac{\partial \psi}{\partial F^e} F^{i-T} - J \Pi F^{-T} \quad (27)$$

and the Cauchy stress is obtained from Eq. (12):

$$\sigma = J^{-1} \frac{\partial \psi}{\partial F^e} F^{eT} - \Pi \mathbf{1} \quad (28)$$

We assume local chemical equilibrium with respect to the absorption of water, giving the state law for the chemical potential:

$$\mu = \frac{\partial \psi}{\partial C} + pv \quad (29)$$

Finally, the inequality (25) identifies the driving force for chemical degradation as:

$$\omega := p f' - \frac{\partial \psi}{\partial \zeta} \quad (30)$$

where  $-\frac{\partial \psi}{\partial \zeta}$  is called the chemical affinity (Ulm et al., 2000; Loeffel and Anand, 2011). The inequality finally reduces to:

$$\omega \dot{\zeta} - J \cdot \nabla \mu \geq 0 \quad (31)$$

Kinetic models for the extent of reaction and diffusion of water should be such that the inequality (31) is satisfied.

## 4. Constitutive theory

### 4.1. Free energy function

We assume that the Helmholtz free energy  $\psi$  can be additively decomposed as follows:

$$\psi = \mu_0 C + \psi_{mech} + \psi_{mix} + \psi_{reac} \quad (32)$$

where  $\psi_{mech}$  is the free energy of stretching the network,  $\psi_{mix}$  is the free energy of mixing polymer and water, and  $\psi_{reac}$  represents the potential energy of chemical reaction. The first term defines  $\mu_0$  as the reference chemical potential of pure water.

The stretching free energy is further decomposed as:

$$\psi_{mech}(\mathbf{F}^e, C, \zeta) = (1-f)\tilde{\psi}(\tilde{\mathbf{C}}, \zeta) \quad (33)$$

where the  $(1-f)$  pre-factor represents the ratio of remaining polymer to initial polymer volume and  $\tilde{\psi}$  represents the stretching free energy per unit volume in the dry, degraded configuration. Deformations are then measured relative to dry state of the degraded network through the tensor  $\tilde{\mathbf{F}}$  accounting for swelling and elastic distortion of the degraded network:

$$\tilde{\mathbf{F}} = (1 + \nu\tilde{\mathbf{C}})^{1/3} \mathbf{F}^e = (1-f)^{-1/3} \mathbf{F} \quad (34)$$

where we recall that  $\tilde{\mathbf{C}} = \mathbf{C}/(1-f)$  is the number of water molecules per unit volume in the dry degraded state. The corresponding right Cauchy–Green tensor is given by  $\tilde{\mathbf{C}} := \tilde{\mathbf{F}}^T \tilde{\mathbf{F}}$ , and its invariants are denoted  $\tilde{I}_i$ ,  $i = 1, 2, 3$ . At this point, any model of rubber elasticity expressed in terms of the invariants of the right Cauchy–Green tensor can be used for  $\tilde{\psi}$ . Here, we adopt the phenomenological Gent model (Gent, 1996), which captures strain-stiffening of the network at large deformations. The Gent model applied to the degrading polymer network is expressed as:

$$\tilde{\psi}^G(\tilde{I}_1, \zeta) = -\frac{GJ_m}{2} \ln \left( 1 - \frac{\tilde{I}_1 - 3}{J_m} \right) \quad (35)$$

where  $G$  is the shear modulus of the dry, degraded network and  $J_m$  is a fitting parameter representing the limiting value of  $\tilde{I}_1$ . In general, both  $G$  and  $J_m$  depend on the degradation state. However, in the following we will neglect the effect of degradation on  $J_m$ , since strain-stiffening will be found to play a negligible role on our results. Expressions for  $G(\zeta)$  will be developed later for specific model hydrogels. In the limit of small stretches, the Gent model (35) reduces to the neo-Hookean model:

$$\tilde{\psi}^{NH}(\tilde{I}_1, \zeta) = \frac{G}{2} (\tilde{I}_1 - 3) \quad (36)$$

All the results presented in this work were obtained using the Gent model, unless otherwise indicated.

We estimate the free energy of mixing  $\psi_{mix}$  using the Flory–Huggins theory (Flory, 1942; Huggins, 1942):

$$\psi_{mix}(C, \zeta) = \frac{k_B T}{v} J^i [(1-\phi) \ln(1-\phi) + \chi \phi(1-\phi)] \quad (37)$$

where  $k_B$  is the Boltzmann constant,  $T$  is the absolute temperature,  $\phi$  is the volume fraction of polymer defined in Eq. (3), and  $\chi$  is the interaction parameter, which characterises the dis-affinity between the solvent and polymer. Note that in Eq. (37) we have neglected the contribution of the long polymer chains to the entropy of mixing. Here we take the  $\chi$ -parameter as a function of the polymer volume fraction:  $\chi = \chi(\phi)$ . A linear dependency is found to be sufficient for our purpose:  $\chi = \chi_1 + \chi_2 \phi$ , where  $\chi_1$  and  $\chi_2$  are fitting constants.

The chemical reaction energy  $\psi_{reac}$  represents the energy released during hydrolysis and contributing to the driving force for reaction, cf. Eq. (30). To the best of our knowledge, a physically-based expression for the free energy of hydrolytic reaction is not available. Therefore, for simplicity a simple quadratic expression is adopted:

$$\psi_{reac}(\zeta) = \frac{h}{2} (1 - \zeta)^2 \quad (38)$$

where  $h$  is a chemical modulus, treated as a fitting parameter. This expression gives a chemical affinity that is linear in the extent of reaction. As shown below, when combined with a linear kinetic model, this results in overall first-order reaction kinetics (Ulm et al., 2000), which satisfyingly describes the degradation kinetics in hydrogels considered in this work. Note that a quadratic reaction energy has been used in other works addressing chemical reactions in solids, see e.g. Loeffel and Anand (2011), Konica and Sain (2020), Hajikhani et al. (2021).

#### 4.2. State laws

Using Eqs (32)–(34) into the state law (28), we obtain the general expression for the Cauchy stress (assuming that  $\tilde{\psi}$  depends on  $\tilde{I}_1$  only):

$$\boldsymbol{\sigma} = \frac{2}{\lambda_s} \frac{\partial \tilde{\psi}}{\partial \tilde{I}_1} \mathbf{B}^e - p \mathbf{1} \quad (39)$$

where  $\mathbf{B}^e = \mathbf{F}^e \mathbf{F}^{eT}$  is the elastic left Cauchy Green tensor. For the Gent model (35), it particularises as:

$$\boldsymbol{\sigma}^G = G_s \frac{1}{1 - \frac{\tilde{I}_1 - 3}{J_m}} \mathbf{B}^e - p \mathbf{1} \quad (40)$$

while for the Neo–Hookean model it reduces to:

$$\boldsymbol{\sigma}^{NH} = G_s \mathbf{B}^e - p \mathbf{1} \quad (41)$$

In Eqs (40) and (41),  $G_s := G/\lambda_s = G\phi^{1/3}$  represents the swollen modulus of the hydrogel. Under the assumption of elastic incompressibility, the Young modulus in the degraded dry and swollen states are respectively given by  $E = 3G$  and  $E_s = 3G_s$ .



Using Eqs (32)–(34) and (37) into the state law for the chemical potential (29), we obtain:

$$\mu = \mu_0 + k_B T [\ln(1 - \phi) + \phi + (\chi_1 - \chi_2)\phi^2 + 2\chi_2\phi^3] + \Pi v \quad (42)$$

When the  $\chi$  parameter is constant, the usual expression is recovered:

$$\mu = \mu_0 + k_B T [\ln(1 - \phi) + \phi + \chi\phi^2] + \Pi v \quad (43)$$

Finally, using Eqs (32)–(34), (37) and (38), the reaction driving force (30) is obtained:

$$\omega = \omega_c + \omega_f + \omega_g \quad (44)$$

where:

$$\begin{aligned} \omega_c &:= h(1 - \zeta) \\ \omega_f &:= \left[ \Pi - \frac{2}{3} \frac{\partial \tilde{\psi}}{\partial \tilde{I}_1} \bigg|_{\zeta} \tilde{I}_1 + \tilde{\psi} - \frac{kT}{v} (1 - \phi)(1 - \chi_1(1 - \phi) - 2\chi_2\phi(1 - \phi)) \right] f' \\ \omega_g &:= -(1 - f) \frac{\partial \tilde{\psi}}{\partial \zeta} \bigg|_{\tilde{I}_1} \end{aligned} \quad (45)$$

The first term  $\omega_c$  is the direct contribution from the energy of reaction. The second term  $\omega_f$  represents coupled effects resulting from polymer mass loss. This term includes the effect of hydrostatic stress due to the related volume change, and the change in elastic energy and mixing energy due to mass loss. The third term  $\omega_g$  represents the coupled effect due to change in network structure (and thus elastic modulus), independent of mass loss.

#### 4.3. Kinetic models

We satisfy the inequality (31) by requiring that the contributions of degradation and diffusion are both non-negative via the kinetic models. The simplest kinetic model for degradation is to take the degradation rate to be proportional to the reaction driving force:

$$\dot{\zeta} = \begin{cases} k\omega & \omega \geq 0 \\ 0 & \text{otherwise} \end{cases} \quad (46)$$

where  $k$  is positive and may in general depend on composition. Here,  $k$  is assumed constant for simplicity. The degradation rate is set to zero for negative values of  $\omega$  because the hydrolysis reaction is irreversible.

Under conditions where the coupled contributions  $\omega_f$  and  $\omega_g$  to the chemical driving force (44) are much smaller than the direct contribution  $\omega_c$ , the kinetic model (46) reduces to  $\dot{\zeta} = k'(1 - \zeta)$ , where  $k' := kh$ . This is similar to a first-order reaction kinetic model with rate constant  $k'$  (Ulm et al., 2000). The evolution of the degradation variable with time is then described by a simple exponential relation:

$$\zeta(t) = 1 - \exp(-k't) \quad (47)$$

In this case, the only determining parameter is  $k'$ , while individual values of the chemical modulus  $h$  and kinetic parameter  $k$  are irrelevant as far as the time evolution of the degradation state variable is concerned. Past studies have suggested that hydrogels degrading by hydrolysis follow a first-order reaction kinetic model (Metters et al., 2000b; Li et al., 2011). As shown below, this is also the conclusion of the present work. Note however that, different from previous studies, coupled contributions to the reaction driving forces are not neglected a priori, but instead will be found to be negligible as a result of the model calibration process.

The simplest kinetic model for the diffusion of water molecules is:

$$\mathbf{J} = -M \cdot \nabla \mu \quad (48)$$

where  $M$  is a constant mobility coefficient. Inserting (48) into the conservation Eq. (13), and assuming pseudo steady state, it follows that the field of chemical potential must satisfy the Laplace equation, together with boundary conditions. In the following, we will only consider examples where the chemical potential is uniform throughout the gel.

### 5. Application 1: Near-ideal Tetra-PEG hydrogels

As a first application of the theory, we consider Tetra-PEG hydrogels first introduced by Sakai and co-workers as a model (near-)ideal polymer network with homogeneous network structure and uniform chain length (Sakai et al., 2008). Tetra-PEG hydrogels are produced by the AB-type coupling of two types of four-arm polyethylene glycol (PEG) macromolecules functionalised with mutually reactive end groups in solution. The reaction probability can be measured, and even tuned, providing a high degree of control on their network structure (Nishi et al., 2012, 2017). Therefore, near-ideal Tetra-PEG hydrogels constitute systems of choice to assess theories of rubber elasticity.

Li et al. (2011) have extended the concept of Tetra-PEG hydrogel by implementing tunable degradability. These authors considered three types of four-arm PEG macromolecules mixed in stoichiometric proportion, namely Tetra-PEG–OSu (TAPEG), Tetra-PEG–NH<sub>2</sub> (TCPEG), and Tetra-PEG–deg-OSu (TGPEG). The latter contains a cleavable ester bond. TAPEG can react with both TCPEG and TGPEG. The ratio of the amount of TGPEG to the total amount of TCPEG and TGPEG,  $r_{deg}$ , gives the fraction of cleavable links



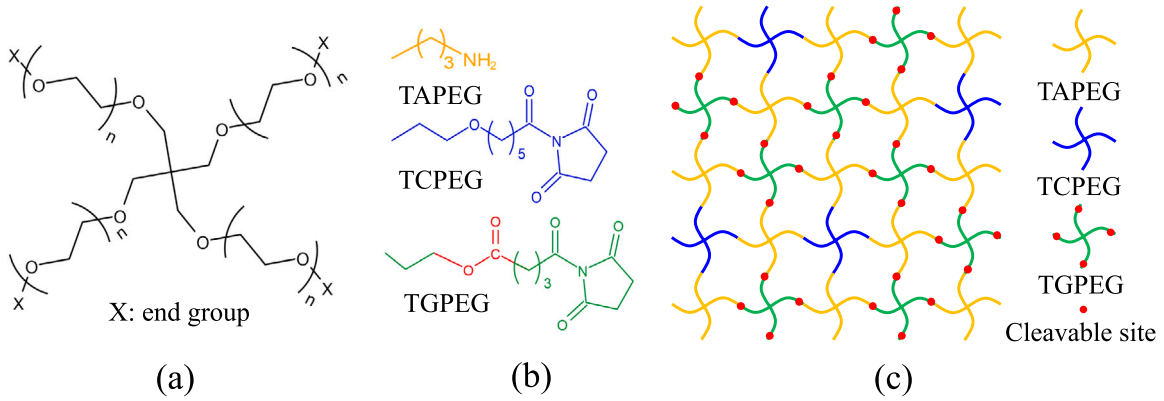


**Fig. 3.** Schematic structure of degradability-tunable Tetra-PEG hydrogels. (a) Chemical structure of a functionalised Tetra-PEG hydrogel macromolecule, (b) the end group structures of TAPEG, TCPEG, and TGPEG, and (c) the network structure resulting from the cross-coupling of the macromolecular precursors.

in the formed network, and can be used to tune the degradability of the hydrogel. The Tetra-PEG macromolecules and resulting network structure are illustrated in Fig. 3.

We define the average connectivity  $\rho$  as the fraction of connected arms in the network. In the initial, as-prepared state,  $\zeta = 0$  and  $\rho = \rho_0$ , where  $\rho_0$  is the conversion ratio of the macromolecular precursors. Since there is a maximum of one cleavable link per polymer strand between junctions, the average connectivity  $\rho$  of the degrading network can be related to the degradation state variable  $\zeta$  by:

$$\rho = \rho_0 [(1 - r_{deg}) + (1 - \zeta)r_{deg}] \quad (49)$$

where we have accounted for the fact that only a fraction  $r_{deg}$  of the links can be broken. This relation recovers  $\rho = \rho_0$  for  $\zeta = 0$ , as required.

In the following, we first propose physically-based models for the dry shear modulus and mass loss fraction in terms of connectivity, and thus degradation state via Eq. (49). We then use the proposed models together with the complete thermodynamic framework presented in the previous section to simulate concurrent swelling and degradation of these gels and we compare theoretical predictions to experimental data reported by Li et al. (2011).

### 5.1. Degraded modulus

We relate the shear modulus of the dry network to the (evolving) network topology using the classical Phantom model (Graessley, 1975; Flory, 1976):

$$G^{Ph} = \xi N_p kT \quad (50)$$

where  $N_p$  is the number density of four-arm macromolecular precursors and  $\xi$  is the cycle rank of the network per precursor. The cycle rank represents the number of chains that need to be cut in order to reduce the network to a tree with no closed cycle. It can be expressed as  $\xi = \nu - \nu$ , where  $\nu$  and  $\nu$  are the numbers of elastically effective chains and crosslinks per precursor, respectively (Mark and Erman, 2007). The latter can in turn be expressed in terms of the average connectivity  $\rho$  based on tree-like theory (Miller and Macosko, 1976; Rubinstein and Colby, 2003), which is recalled in the following.

Consider an infinite Bethe lattice (or Cayley tree) representing a network formed from  $z$ -functional macromolecular precursors. Each ('parent') lattice site has thus  $z$  possible paths to other sites: one 'grandparent' site and  $(z-1)$  'child' sites. Consider an arbitrary bond between two lattice sites, and introduce  $P_\infty$  as the probability that this bond does *not* lead to infinity. This can happen either because the bond itself has not formed (or has been hydrolysed), or because none of its  $z-1$  appended bonds lead to infinity. Therefore,  $P_\infty$  is given by the following recursive formula:

$$P_\infty = (1 - \rho) + \rho(P_\infty)^{z-1} \quad (51)$$

For Tetra-PEG gels,  $z = 4$ , and Eq. (51) can be solved for  $P_\infty$ :

$$P_\infty = -\frac{1}{2} + \left(\frac{1}{\rho} - \frac{3}{4}\right)^{1/2} \quad (52)$$

The probability  $P_\infty$  is used to estimate the density of elastically effective chains and crosslinks. In the tree representation, an effective crosslink is defined as a junction point between at least three bonds leading to an infinite network, and effective chains are defined as bonds joining two effective crosslinks. The following estimates for  $\nu$  and  $\nu$  are then readily obtained, noting that each chain is shared by two crosslinks (Nishi et al., 2017):

$$\nu = \left[ \frac{3}{2} C_3^4 (1 - P_\infty)^3 P_\infty + \frac{4}{2} C_4^4 (1 - P_\infty)^4 \right] \quad (53)$$

$$v = [C_3^4(1 - P_\infty)^3 P_\infty + C_4^4(1 - P_\infty)^4] \quad (54)$$

The cycle rank per precursor can then be calculated in terms of connectivity probability:

$$\xi = \left( \frac{1}{2} + \left( \frac{1}{\rho} - \frac{3}{4} \right)^{\frac{1}{2}} \right) \left( \frac{3}{2} - \left( \frac{1}{\rho} - \frac{3}{4} \right)^{\frac{1}{2}} \right)^3 \quad (55)$$

Note that, for a (hypothetical) tetra-functional perfect network ( $\rho = 1$ ), we have  $v = 2$ ,  $\nu = 1$  and  $\xi = 1$ .

The applicability of the Phantom model (50) to (non-degradable) Tetra-PEG gels with various  $\rho$ -values has been extensively investigated by Sakai and co-workers (Nishi et al., 2012; Akagi et al., 2013; Nishi et al., 2017; Sakumichi et al., 2021). In brief, these authors found that the Phantom model with cycle rank estimated by tree-like theory, Eq. (55), provides a reasonable estimate of the modulus of  $\rho$ -tuned hydrogels at polymer concentrations close to the overlap concentration, but systematically underestimates the modulus at larger polymer concentrations (Nishi et al., 2017). However, they also found that the Phantom model remarkably well predicts the ratio  $G/G^*$  as a function of connectivity  $\rho$  for a broad range of concentration and connectivity values, where  $G^*$  is the modulus of a perfect network prepared at the same concentration:  $G/G^* \approx \xi(\rho)$ .<sup>1</sup> In this work, we build on these findings and propose that the modulus of the degraded network can be related to the modulus of the initial, undegraded network  $G_0$  by:

$$\frac{G}{G_0} = \frac{\xi(\rho)}{\xi(\rho_0)} \quad (56)$$

where the cycle ranks of the degraded and initial network are estimated from expression (55). When comparing to experimental data, we set the initial modulus  $G_0$  and connectivity  $\rho_0$  to their experimental values and use (56) to predict the degraded modulus in terms of the evolving connectivity probability  $\rho$ . The latter can in turn be related to the degradation state by Eq. (49).

As an illustration, the ratio  $G/G_0$  is plotted as a function of the average connectivity  $\rho$  in Fig. 4(a) (right y-axis), for two values of initial connectivity probability:  $\rho_0 = 1$  and  $\rho_0 = 0.86$ . For large connectivity values, the normalised modulus decreases approximately linearly as connectivity decreases. The high connectivity behaviour is well described by an Effective Medium Approximation (EMA) for tetra-functional networks (Nishi et al., 2012, 2017):

$$\frac{G}{G_0} \approx \frac{2\rho - 1}{2\rho_0 - 1} \quad (57)$$

Deviations from linearity arise when the connectivity approaches the percolation threshold, which is given by  $\rho_c = 0.33$  according to the Phantom model (56). This is reasonably close to the prediction obtained for a diamond lattice,  $\rho_c = 0.39$  (Stauffer and Aharony, 1994). As shown in the following, accounting for the nonlinear behaviour near the percolation threshold is important to capture the experimental trends up to reverse gelation. The same ratio  $G/G_0$  is plotted as a function of the extent of reaction  $\zeta$  in Fig. 4(b) (right y-axis). Note that the critical value  $\zeta_c$  corresponding to a vanishing modulus depends on the initial connectivity.

## 5.2. Mass loss

Our model for mass loss closely follows a classical model proposed to predict the sol fraction resulting from gelation (Rubinstein and Colby, 2003). Indeed, degradation can be regarded as a reverse gelation process. In a Bethe lattice, the sol fraction relative to the total polymer mass is given by the fraction of lattice sites that are not connected to the infinite network through any of its four potential bonds,  $(P_\infty)^4$ . The mass loss fraction  $f$ , however, is defined with respect to the initial polymer mass, assuming that the initial sol fraction has migrated out of the gel, so that  $f = 0$  when  $\rho = \rho_0$ . We therefore need to subtract the sol fraction resulting from the gelation process, and to normalise by the initial mass, leading to:

$$f = \frac{(P_\infty)^4 - (P_{\infty 0})^4}{1 - (P_{\infty 0})^4} \quad (58)$$

where  $P_{\infty 0} := P_\infty(\rho_0)$  and  $P_\infty$  is given by Eq. (52). In the case where the network is perfect prior to degradation,  $\rho_0 = 1$ ,  $P_{\infty 0} = 0$  and we recover the original model  $f = (P_\infty)^4$ .

The mass loss fractions  $f$  as a function of the average connectivity  $\rho$  and the extent of reaction  $\zeta$  are shown in Figs. 4(a) and (b) (left y-axis), respectively. We observe that the  $f - \rho$  curves almost overlap each other, because  $(P_{\infty 0})^4$  is small. In contrast, the  $f - \zeta$  curves for two different values of  $\rho_0$  are shifted with respect to each other, because  $\zeta = 0$  corresponds to different values of  $\rho_0$ . In addition, the mass loss fraction  $f$  is negligible when the connectivity is larger than  $\sim 0.8$ , which is because the release of a macromolecular precursor requires losing connectivity through all of the four branches that connect it to the remaining network. Thus, while the modulus ratio  $G/G_0$  drops linearly as soon as degradation starts and the average connectivity decreases, mass loss becomes significant only when the connectivity becomes sufficiently small.

<sup>1</sup> These findings were recently rationalised by Sakumichi et al. (2021), by taking into account a newly-discovered energetic contribution to the shear modulus of Tetra-PEG hydrogels, which was found to depend on polymer concentration and precursor molecular weight, see also Yoshikawa et al. (2021). Normalising the modulus by the modulus of the corresponding perfect network suppresses the dependency on concentration and precursor molecular weight. This ratio was further shown to be remarkably well described by the cycle rank  $\xi(\rho)$  estimated under the Bethe lattice approximation (Sakumichi et al., 2021).

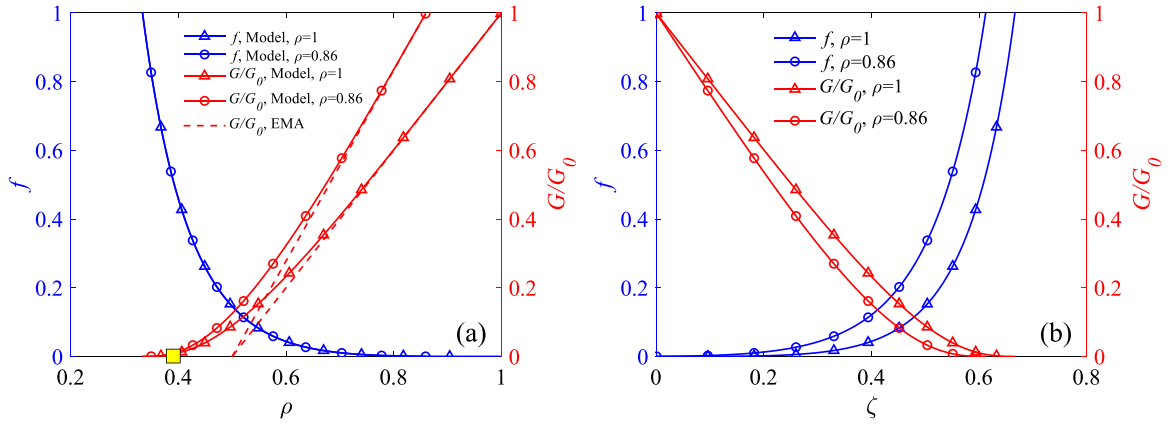


**Fig. 4.** (a) Normalised mass loss  $f$  (left y-axis) and elastic modulus  $G/G_0$  (right y-axis) as functions of (a) the connectivity probability  $\rho$  and (b) the extent of reaction  $\zeta$  for Tetra-PEG hydrogels with different initial connectivity probabilities  $\rho_0$ . Modulus predictions based on tree-like theory are also compared to a linear EMA estimate. The predicted percolation threshold is close to that of a diamond lattice represented by the yellow square marker.

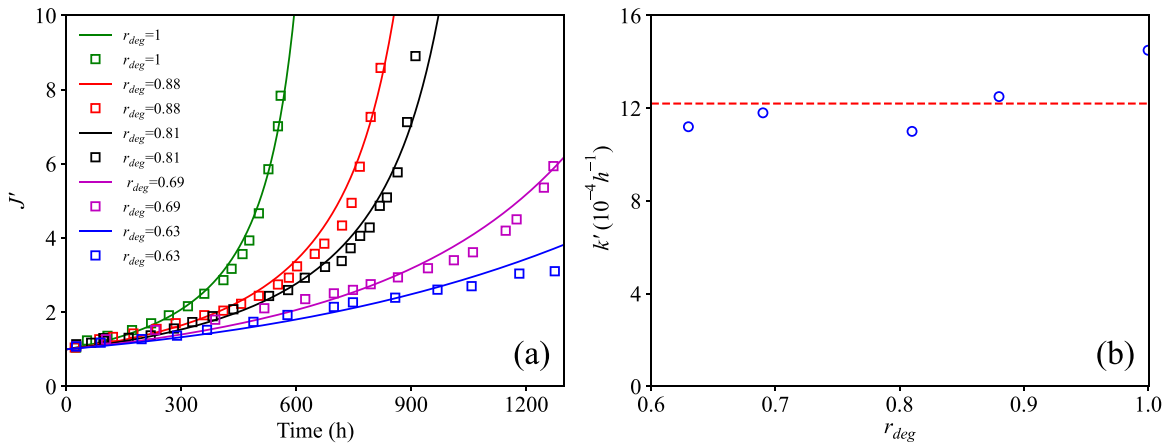


**Fig. 5.** (a) Normalised swelling ratio  $J'$  as a function of time for Tetra-PEG hydrogels with different fractions of degradable units  $r_{deg}$ . The symbols denote the experimental data, while the lines represent the model predictions. (b) Fitted rate constant  $k'$  for different values of  $r_{deg}$ . The red dashed line represents the average value of  $r_{deg}$ .

### 5.3. Free swelling conditions

Under the conditions of free swelling, we have  $\mathbf{F} = \lambda^s \lambda^d \mathbf{1}$ ,  $\mathbf{B}^e = \mathbf{1}$ , and the hydrostatic pressure  $\Pi$  is easily identified using the boundary conditions  $\sigma_{11} = \sigma_{22} = \sigma_{33} = 0$  in the state law (39):

$$\Pi = \frac{2}{\lambda_s} \frac{\partial \tilde{\psi}}{\partial \tilde{I}_1} \quad (59)$$

Assuming fast diffusion of water, the chemical potential of water is uniform throughout the gel, and is equal to the chemical potential of pure water:  $\mu = \mu_0$ . For Tetra-PEG hydrogels, we found a good agreement with experimental data by considering a constant  $\chi$ -parameter in the expression of the chemical potential. Inserting Eq. (59) into Eq. (43), the free swelling condition is obtained:

$$k_B T [\ln(1 - \phi) + \phi + \chi \phi^2] + \frac{2}{\lambda_s} \frac{\partial \tilde{\psi}}{\partial \tilde{I}_1} v = 0 \quad (60)$$

which is nothing but the Flory–Rehner condition (Flory and Rehner, 1943), here generalised to a degrading gel with elastic free energy written as a general function of  $\tilde{I}_1$ . This condition states that the equilibrium concentration of water at a given time results from the competition between entropy of mixing (which favours water absorption) and the elastic stretching of the polymer network (which resists water absorption). For a given degradation state  $\zeta$ , Eq. (60) can be solved for the polymer volume fraction  $\phi$ , and the equilibrium water concentration is in turn found from relation (3).

To calculate the evolution of the degradation variable  $\zeta$  over time, the reaction driving force (44) is calculated for the current state, and the corresponding reaction rate is calculated using the kinetic model (46). Here, for simplicity, the rate equation is discretised in time using a backward Euler scheme and the extent of reaction at the next time step is calculated explicitly.

**Table 1**

Material parameters for degradable Tetra-PEG hydrogels.

Parameter	Unit	$r_{deg} = 1$	$r_{deg} = 0.88$	$r_{deg} = 0.81$	$r_{deg} = 0.69$	$r_{deg} = 0.63$	Reference
$k_B$	J K <sup>-1</sup>	$1.38 \times 10^{-23}$	$1.38 \times 10^{-23}$	$1.38 \times 10^{-23}$	$1.38 \times 10^{-23}$	$1.38 \times 10^{-23}$	Commonly known
$\nu$	m <sup>3</sup>	$3 \times 10^{-29}$	$3 \times 10^{-29}$	$3 \times 10^{-29}$	$3 \times 10^{-29}$	$3 \times 10^{-29}$	Commonly known
$T$	K	310	310	310	310	310	Li et al. (2011)
$\chi$	–	0.45	0.45	0.45	0.45	0.45	Li et al. (2011)
$G_0$	kPa	26.5	27.3	28.6	26.1	27.3	Li et al. (2011)
$J_m$	–	1000	1000	1000	1000	1000	Fitted
$k'$	h <sup>-1</sup>	$1.45 \times 10^{-3}$	$1.25 \times 10^{-3}$	$1.10 \times 10^{-3}$	$1.18 \times 10^{-3}$	$1.12 \times 10^{-3}$	Fitted

#### 5.4. Comparison to experimental data

Fig. 5(a) shows the normalised swelling ratio  $J' := J/J_0$  as a function of time for Tetra-PEG hydrogels prepared with different fractions of degradable units  $r_{deg}$ . Here,  $J = J'$  is the swelling ratio measured relative to the reference volume, Eq. (8), and  $J_0$  is the corresponding swelling ratio before the onset of degradation, i.e. the swelling ratio of the undegraded network. Note that  $J = (1 - f)Q$ , where  $Q$  is the swelling ratio measured with respect to the dry degraded state, Eq. (4). Experimental data are taken from Li et al. (2011).<sup>2</sup> The material parameters used in the model are collected in Table 1. All parameters values are either commonly known or taken from Li et al. (2011), except for the maximum extensibility parameter  $J_m$ , the chemical modulus  $h$ , and the kinetic coefficient  $k$ . Here, a constant value of chemical modulus  $h = 50$  GPa was used, while the parameter  $k$  was fitted separately for each curve. Note that we only report the product  $k' = kh$  in the table, because the model here operates under conditions of first order reaction kinetics, see Section 4.3. An excellent agreement is observed between the model predictions and experimental data for all the samples.

Fig. 5(b) shows the rate constant  $k' = kh$  calibrated on the experimental data. Remarkably, the calibrated values of  $k'$  are approximately the same in samples with different  $r_{deg}$  fractions. The average value of  $k'$  is  $1.23 \times 10^{-3} \text{ h}^{-1}$ , also shown in the figure by the red dashed line. This value is very close to the value obtained by Li et al. (2011) based on Flory–Rehner equation (neglecting mass loss) combined with the Phantom model for the shear modulus, and assuming a first-order kinetics for the connectivity.

Model predictions of the time evolution of the extent of reaction  $\zeta$  are shown in Fig. 6(a) together with the prediction of the first-order kinetic model (47), using the average fitted  $k'$  value, confirming that damage evolution is approximately described by an exponential. Figs. 6 (b) and (c) show model predictions for the dry shear modulus and mass loss fraction. As expected for these gels, the shear modulus drops as soon as degradation starts as a result of a decrease in average connectivity, while the mass loss fraction  $f$  remains small at the beginning of the degradation process but rises rapidly afterwards. Note that Li et al. (2011) did not provide direct experimental measurements for the modulus and mass loss fraction.

We verify that our model indeed reduces to a first-order kinetic model of degradation under the conditions of free swelling. Fig. 7(a) shows the relative contributions of each term in the reaction driving force as a function of time, for two different values of the chemical modulus  $h$ . For the value of  $h$  used to fit the data ( $h = 50$  GPa, continuous lines), the coupled terms are negligible in comparison to the direct contribution  $\omega_c$ . In this case, the kinetic model of degradation reduces to the first-order reaction kinetic model Eq. (47), dictated by the rate constant  $k'$ . In contrast, when  $h$  is set to a much smaller value ( $h = 0.5$  GPa, dashed lines), the contributions of the coupling term  $\omega_f$  associated to mass loss significantly decreases the total reaction driving force during degradation. The corresponding normalised swelling ratio is shown as a function of time in Fig. 7(b), in the case  $r_{deg} = 0.81$  and for these two  $h$ -values. Here, we used the same value of  $k'$  in both cases, and calculated  $k$  accordingly. We observe that using a small value of  $h$  (small enough for the coupled effects to become significant) does not allow us to reproduce the experimental trends, despite the larger value of  $k$ . This confirms that coupled effect are negligible in driving the degradation reaction, and that degradation overall obeys a first-order kinetics.

The effect of the maximum extensibility parameter  $J_m$  of the Gent model on the predicted swelling ratio is illustrated in Fig. 8 for a Tetra-PEG gel with  $r_{deg} = 1$ . Our results suggest that the extensibility limit does not play a dominant role on the swelling response (as long as it is sufficiently large), and further that using the neo–Hookean model would give satisfying predictions (noting that the Gent model reduces to the neo–Hookean model for  $J_m \rightarrow \infty$ ). In our model, the extensibility parameter was assumed constant during the entire degradation process. We note that this is unlikely to be the case in reality. For example, previous numerical simulations using random discrete networks show that the extensibility limit increases as the network connectivity decreases (Alamé and Brassart, 2020). However, for the free swelling of degrading Tetra-PEG gels, our results suggest that the network stretch remains far from the extensibility limit at all times, and therefore capturing the precise evolution of the extensibility limit with degradation state appears not to be necessary.

Fig. 8 also shows model predictions obtained by combining the Gent model with the EMA model for the shear modulus, Eq. (57). The EMA model largely overestimates the percolation threshold, cf. Fig. 4, see also Nishi et al. (2012), Alamé and Brassart

<sup>2</sup> In their paper, Li et al. (2011) define  $J'$  as “the ratio of the gel volume in the equilibrium-swollen state to that in the as-prepared state”. We think that the gel volume in the as-prepared state should be understood as the volume of the undegraded hydrogel under free swelling condition, giving indeed  $J'(0) = 1$ . Using the gel volume “in the as-prepared state” would give  $J'(0) < 1$ , since hydrogels formed in solution are not in a state of swelling equilibrium at the polymer preparation concentration.

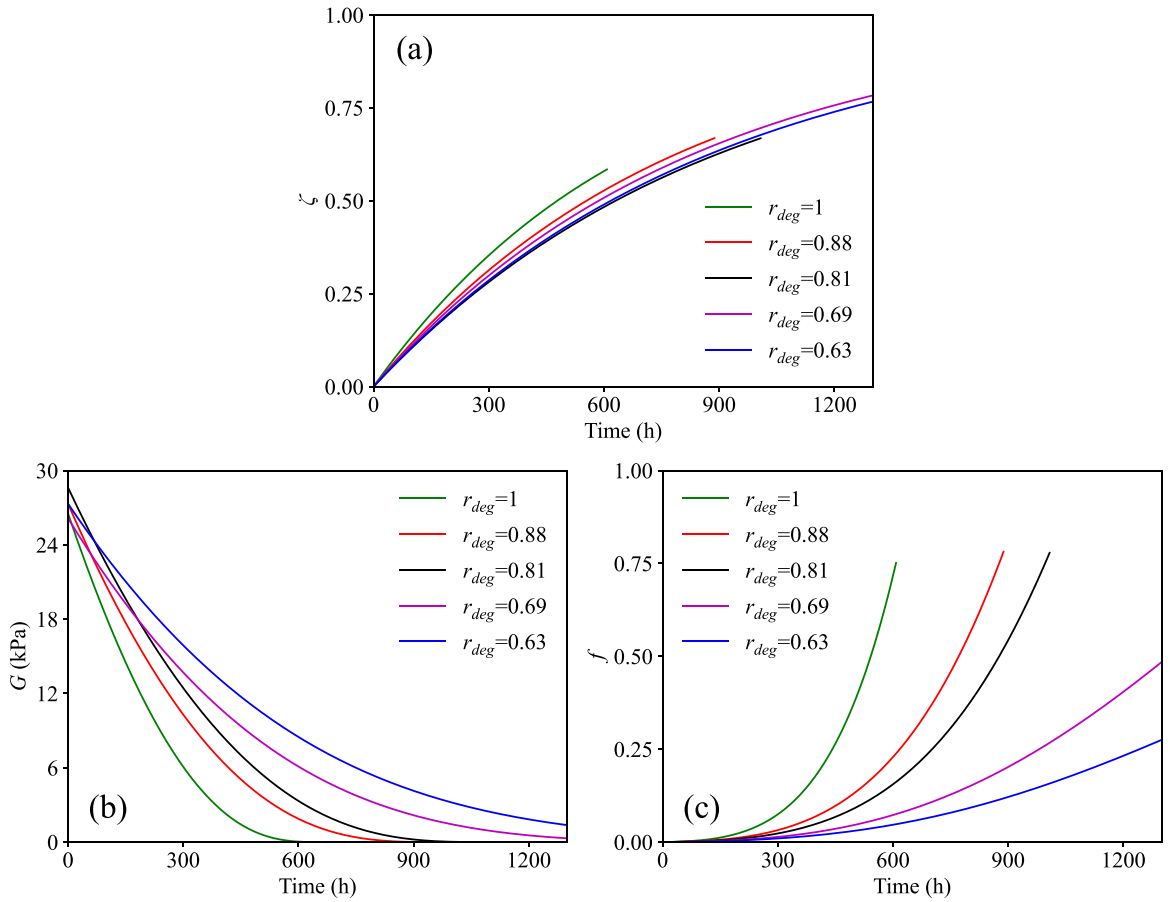


Fig. 6. Model predictions of time evolution for (a) extent of reaction  $\zeta$ , (b) shear modulus  $G$  and (c) mass loss  $f$  for Tetra-PEG hydrogels with different fractions of degradable units  $r_{deg}$ . In (a) the predictions of the simple first-order kinetic model (47) are also shown, using the average of the fitted  $k'$ .

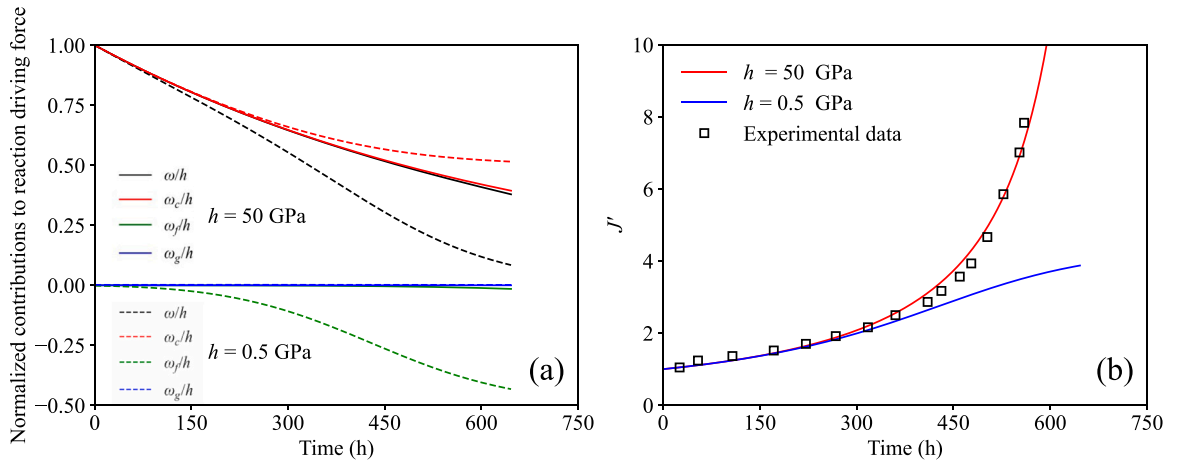
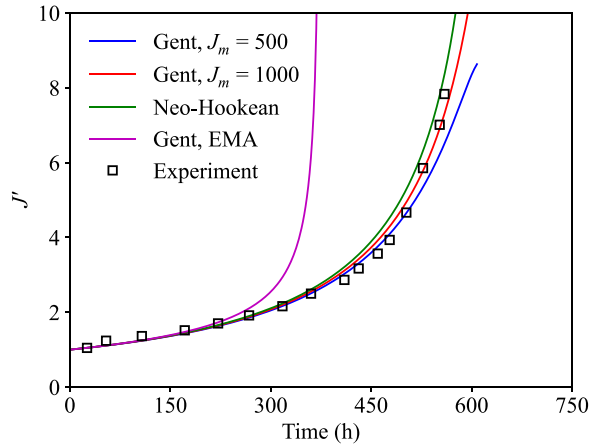
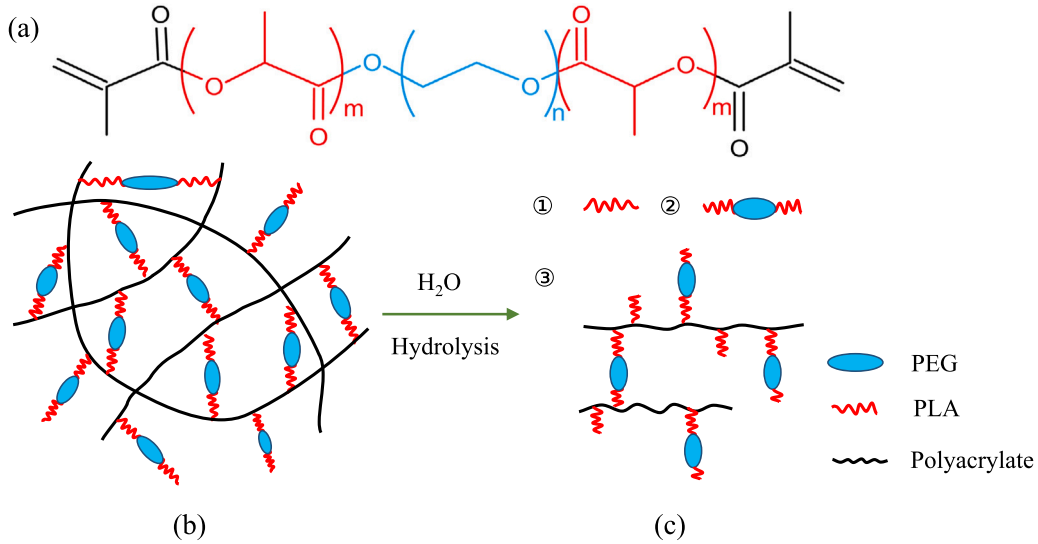


Fig. 7. Effect of the chemical modulus  $h$  on the time evolution of (a) normalised contributions to the reaction driving force (44), and (b) normalised swelling ratio  $J'$ .

(2020), and in turns predicts the reverse gelation point too early. This shows that capturing the nonlinear evolution of modulus as the degrading network approaches its percolation threshold is critical to obtain a good agreement with experiments up to final degradation.



**Fig. 8.** Normalised swelling ratio  $J'$  as a function of time for a Tetra-PEG hydrogel with  $r_{deg} = 1$ . Comparison between the Gent and neo-Hookean model, with shear modulus predicted by the Phantom model. Predictions are also shown for the Gent model ( $J_m = 1000$ ) with modulus predicted by EMA, Eq. (57).



**Fig. 9.** Schematic structure of the PLA-b-PEG-b-PLA hydrogel and its degradation products. (a) Chemical structure of the PLA-b-PEG-b-PLA macromonomer functionalised with acrylate end-groups, (b) Schematic of the network structure formed by crosslinking of the polyacrylate chains, and (c) the degradation products.

## 6. Application 2: PLA-b-PEG-b-PLA hydrogels

As a second example, we consider poly(lactic acid)-co-poly(ethylene glycol)-co-poly(lactic acid) (PLA-b-PEG-b-PLA) hydrogels considered by Metters and co-authors (Metters et al., 2000a,b, 2001b). The block copolymer precursor consists of a central hydrophilic PEG block with  $n$  ethylene glycols units, flanked with  $m$  lactide units (and thus  $m$  cleavable ester bonds) on each side. The ratio of PEG to PLA segments can be used to tune the mechanical and degradation properties, making these hydrogels attractive for cell encapsulation studies (Diederich et al., 2017). Crosslinked networks are formed by photo-polymerising the tri-block copolymers functionalised with acrylate end-groups, resulting in long polyacrylate (PAA) chains bridged by PLA-b-PEG-b-PLA acting as cross-links. In the following, we will use the following notation: “molecular weight of the PEG chain” - “average number of lactide repeat units on each end” to describe the chemical structure of the PLA-b-PEG-b-PLA macromonomers. For example, the notation 4000 – 10 denotes a macromonomer containing a 4000 Da PEG chain with an average of 10 lactide repeat units on each side. The chemical formulation of the macromonomer, the schematic of the network structure, and the degradation products are shown in Fig. 9.

### 6.1. Degraded modulus

We propose an expression for the degraded dry modulus  $G$  in PLA-b-PEG-b-PLA hydrogels based on the Phantom model under the tree-like approximation, following steps similar to Section 5.1. First define  $p_e$  as the probability that any random ester bond has reacted. In a mean-field approximation,  $p_e$  equals the extent of reaction  $\zeta$ :

$$p_e = \zeta \quad (61)$$

The probability that any PLA segment has been cut is then given by

$$p_s = 1 - (1 - \zeta)^m \quad (62)$$

The average connectivity  $\rho$  here corresponds to the probability that a PLA-b-PEG-b-PLA cross-link is connected to the network on both sides, and is given by:

$$\rho = (1 - p_s)^2 = (1 - \zeta)^{2m} \quad (63)$$

We consider the tree-like representation of the polymer network. Here, each PLA-b-PEG-b-PLA cross-link connects two long PAA chains, which cannot be hydrolysed. Consequently, the recurrence relation for the probability that an arbitrary branch does not lead to infinity is expressed as:

$$P_\infty = (1 - \rho) + \rho(P_\infty)^{N-1} \quad (64)$$

where  $N$  is the number of PLA-b-PEG-b-PLA cross-links attached to one PAA chain. Therefore, the number (per precursor) density of elastically effective chains  $\nu$  and elastically effective crosslinks  $\nu$  are obtained as:

$$\nu = \frac{3}{2} (1 - P_\infty) (1 - (P_\infty)^{N-1}) \quad (65)$$

$$\nu = (1 - P_\infty) (1 - (P_\infty)^{N-1}) \quad (66)$$

Using Eq. (64), Eqs (65)–(66) can be rewritten as

$$\nu = \frac{3}{2} \frac{(1 - P_\infty)^2}{\rho} \quad (67)$$

$$\nu = \frac{(1 - P_\infty)^2}{\rho} \quad (68)$$

These expressions are then used in expression (56), giving:

$$\frac{G}{G_0} = \frac{(1 - P_\infty)^2}{(1 - P_{\infty 0})^2} \frac{\rho_0}{\rho} \quad (69)$$

In the absence of experimental data for the initial connectivity  $\rho_0$ , for simplicity we set  $\rho_0 = 1$ , giving  $P_{\infty 0} = 0$ . The model (69) then further reduces to:

$$\frac{G}{G_0} = \frac{(1 - P_\infty)^2}{\rho} \quad (70)$$

Figs. 11(a) and (b) show the normalised elastic modulus  $G/G_0$  as a function of the connectivity probability  $\rho$  and the extent of reaction  $\zeta$ , respectively, for hydrogels with different numbers  $N$  of PLA-b-PEG-b-PLA crosslinks per PAA chain, and different numbers of lactide units  $m$  per PLA segment. All the  $G/G_0 - \rho$  curves are very well approximated by a simple linear relation  $G/G_0 = \rho$  far above their percolation thresholds, because  $P_\infty$  is small. Deviation from the linear relation arises as  $\rho$  approaches the percolation threshold, which depends on  $N$ . We note that the percolation thresholds predicted by the Phantom model (70) and a classical mean-field model of percolation on a Bethe lattice,  $\rho_c = \frac{1}{N-1}$  (Rubinstein and Colby, 2003) are in a good agreement, as expected. We can also observe that  $m$  does not affect  $\rho_c$ . When it comes to  $G/G_0 \sim \zeta$ , we find that a larger value of  $m$  or a smaller value of  $N$  leads to a smaller  $\zeta_c$ .

### 6.2. Mass loss

We develop a model for mass loss also relying on a tree representation of the network, inspiring from an earlier mass loss model proposed by Metters et al. (2000a, 2001b). These authors proposed a statistical model which required a special treatment to reproduce the dramatic mass loss rate observed during the final stage of degradation. This is because they evaluated the probabilities of degradation at each site without considering the effect of degradation state in the far field region. Instead, our approach based on a tree representation allows capturing these far-field effects and can predict the mass loss until complete degradation without any special treatment.

The model considers two main reaction products contributing to mass loss: (1) PAA chains and (2) PLA-b-PEG-b-PLA blocks. Mass loss due to the release of short chains of pure PLA is neglected since PLA constitutes a small proportion of the overall weight. The release of a PAA kinetic chain requires the cutting of all the paths connecting it with the remaining network as shown in Fig. 10(a).



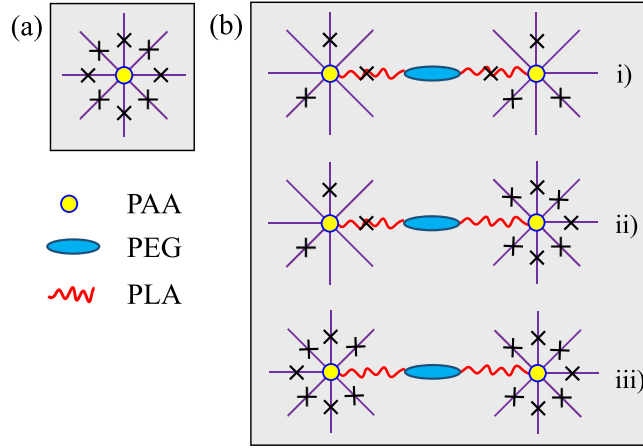


Fig. 10. Schematic representation of the tree-based model for mass loss through the release of (a) PAA chains and (b) PLA-b-PEG-b-PLA segments.

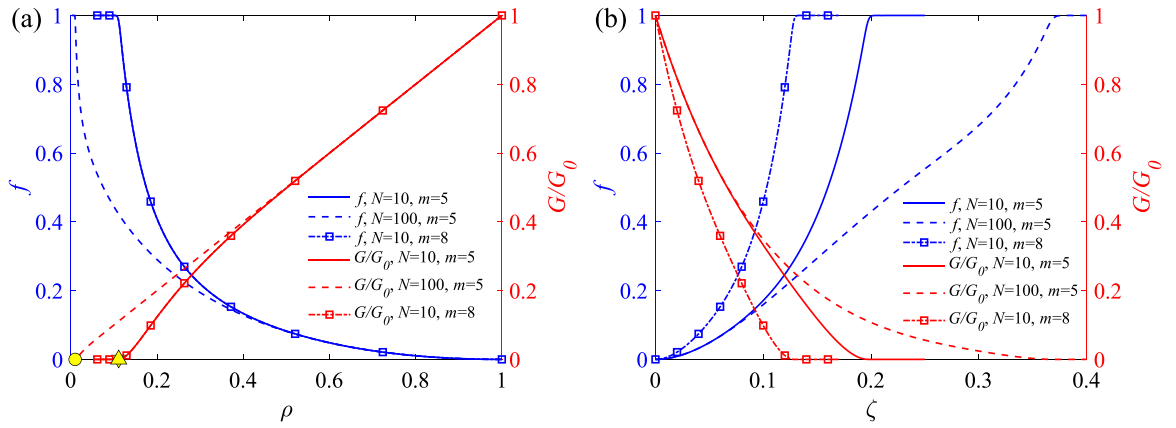


Fig. 11. (a) Normalised mass loss fraction  $f$  (left y-axis) and elastic modulus  $G/G_0$  (right y-axis) as functions of (a) the connectivity probability  $\rho$  and (b) the extent of reaction  $\zeta$  for PLA-b-PEG-b-PLA hydrogels with different cross-links  $N$  and numbers of lactide units  $m$  on each PLA segment. The yellow markers represent the percolation thresholds predicted by the classical mean-field model on a Bethe lattice,  $\rho_c = 1/(N-1)$ .

Note that a PAA chain is condensed into a single site in the diagram for easier understanding, since it cannot be hydrolysed. Assuming that each PAA chain is bonded by  $N$  PLA-b-PEG-b-PLA cross-links, the fraction of the released PAA chains is identified with the probability that none of the  $N$  appended crosslinks connect to infinity:

$$P_{\text{PAA}} = P_{\infty}^N \quad (71)$$

In contrast, a PLA-b-PEG-b-PLA segment can be released via three mechanisms: (i) a single PLA-b-PEG-b-PLA segment is released when both sides are hydrolysed while the PAA chains connecting the block on both sides are connected to the gel through at least one path, (ii) a PLA-b-PEG-b-PLA segment is released when only one of the PAA chains connecting the block is connected to the gel through at least one path and the PLA block on this side must be hydrolysed (regardless of the degradation state of the PLA segment on the other side), and (iii) a PLA-b-PEG-b-PLA is released when neither PAA chain connecting the block is connected to the gel (regardless of the degradation state of the PLA segments on either side of the block). The three mechanisms are illustrated in the tree representation in Fig. 10(b).

The fractions of PLA-b-PEG-b-PLA segments released by the three mechanisms are respectively given by:

$$P_{\text{PEG}}^{(1)} = p_s^2 (1 - (P_{\infty})^{N-1})^2 \quad (72)$$

$$P_{\text{PEG}}^{(2)} = 2 (1 - (P_{\infty})^{N-1}) (P_{\infty})^{N-1} p_s \quad (73)$$

$$P_{\text{PEG}}^{(3)} = (P_{\infty}^{N-1})^2 \quad (74)$$

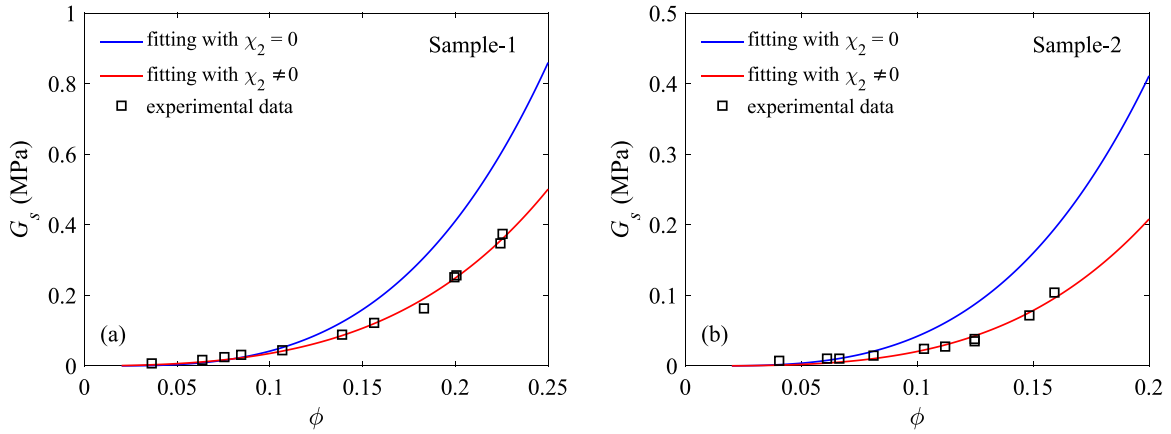


Fig. 12. Fitting of experimental data of  $G_s \sim \phi$  using Eq. (77) with  $\chi_2 = 0$  and  $\chi_2 \neq 0$  for (a) Sample-1 and (b) Sample-2.

Therefore, the total fraction of the released PLA-b-PEG-b-PLA segments is expressed as

$$P_{\text{PEG}} = P_{\text{PEG}}^{(1)} + P_{\text{PEG}}^{(2)} + P_{\text{PEG}}^{(3)} \quad (75)$$

The total mass loss fraction of the hydrogel can then be obtained from the weighted sum as

$$f = w_{\text{PAA}} P_{\text{PAA}} + w_{\text{PEG}} P_{\text{PEG}} \quad (76)$$

where  $w_{\text{PAA}}$  and  $w_{\text{PEG}}$  represent the mass fractions of PAA chains and PLA-b-PEG-b-PLA segments in the hydrogel network. The values of  $w_{\text{PAA}}$ ,  $w_{\text{PEG}}$  can be theoretically calculated for a given macromonomer based on the chemical formula.

Fig. 11(a) and (b) present the  $f - \rho$  and  $f - \zeta$  relations for PLA-b-PEG-b-PLA hydrogels with different values of crosslinks per chain  $N$  and various numbers of lactide units  $m$  on each PLA segment, respectively. Different from the Tetra-PEG gels, the hydrogel starts to lose its mass as soon as degradation starts. The numbers of cross-links  $N$  and lactide units  $m$  both significantly affect the profiles of  $f$  as a function of  $\zeta$ .

### 6.3. Comparison to experimental data

We compare model predictions to experimental data reported for degrading hydrogels prepared with various  $m$ -values and pre-polymer concentrations under free swelling conditions. We note that the parameter  $N$  is not known a priori, but results from the gelation process and is therefore expected to depend on the polymer concentration. For this material, we found necessary to consider a  $\chi$ -parameter that varies linearly with the polymer fraction. In this case the Flory–Rehner relation for free swelling becomes:

$$k_B T [\ln(1 - \phi) + \phi + (\chi_1 - \chi_2)\phi^2 + 2\chi_2\phi^3] + \frac{2}{\lambda_s} \frac{\partial \tilde{\psi}}{\partial I_1} v = 0 \quad (77)$$

The procedure adopted to fit the interaction parameters  $\chi_1$  and  $\chi_2$  is explained below. The maximum extensibility parameter is set to  $J_m = 1000$  like in the previous example. The remaining parameters  $N$  and  $k' = kh$  are calibrated based on experimental data, using the arbitrary value  $h = 50$  GPa and recognising that the process predominantly follows a first-order kinetics.

We first consider hydrogels considered by Metters et al. (2000a), which were polymerised from 4600–5 macromonomers at two different concentrations, namely 50wt% (Sample-1) and 25wt% (Sample-2). Parameters used in the model to reproduce the experimental data are collected in Table 2. The interactions parameters  $\chi_1$  and  $\chi_2$  were obtained by fitting the Flory–Rehner Eq. (77) to experimental  $G_s - \phi$  curves, under the constraint  $G_s > 0$ . The benefit of considering  $G_s - \phi$  curves is that it is independent of the specific kinetic degradation model. The fitting results are presented in Fig. 12(a) and (b) for Sample-1 and Sample-2, respectively. These show that using a constant  $\chi$ -parameter (i.e.  $\chi_2 = 0$ ) cannot give reasonable predictions of the swelling response. In contrast, using a linear variation of  $\chi$  with respect to  $\phi$  can provide an excellent fit to experimental data. The dependence of  $\chi$  on the polymer fraction can probably be ascribed to the fact that the composition can dramatically change during degradation in this kind of material.

The model predictions and experimental results for Sample-1 and Sample-2 are presented in Fig. 13. Fig. 13(a) shows the evolution of the extent of reaction  $\zeta$  with time predicted by the coupled chemo-mechanical model. Predictions obtained using the simplified first-order kinetic model (47) that neglects coupled-field contributions produces virtually indistinguishable results, confirming that first-order kinetics is a good approximation. We also note that the fitted rate constant  $k'$  decreases as polymer concentration increases. In the figure, curves are interrupted at the time where the gel loses all of its mechanical integrity, which is seen to occur at values of  $\zeta$  that are much lower than one in the model.

Figs. 13(b), (c) and (d) show the swollen modulus  $E_s$ , mass loss fraction  $f$  and swelling ratio  $Q = 1/\phi$  (as defined by Eq. (4)), along with experimental values reported by Metters et al. (2000a). As expected, the modulus of hydrogel with the largest initial

**Table 2**  
Material parameters for Sample-1 (50wt%) and Sample-2 (50wt%) (Metters et al., 2000a).

Parameter	Unit	Value (Sample-1)	Value (Sample-2)	Reference
$k_B$	J K <sup>-1</sup>	$1.38 \times 10^{-23}$	$1.38 \times 10^{-23}$	Commonly known
$v$	m <sup>3</sup>	$3 \times 10^{-29}$	$3 \times 10^{-29}$	Commonly known
$w_{PAA}$	–	0.03	0.03	Theoretical value
$w_{PEG}$	–	0.97	0.97	Theoretical value
$T$	K	310	310	Metters et al. (2000a)
$m$	–	5	5	Metters et al. (2000a)
$G_0$	MPa	0.427	0.200	Metters et al. (2000a)
$J_m$	–	1000	1000	Fitted
$\chi_1$	–	0.6061	0.6036	Fitted
$\chi_2$	–	0.1183	0.1022	Fitted
$N$	–	90	20	Fitted
$k'$	min <sup>-1</sup>	$4.0 \times 10^{-5}$	$7.3 \times 10^{-5}$	Fitted

**Table 3**  
Material parameters for samples with 10wt% (Diederich et al., 2017).

Parameter	Unit	Value ( $m = 2$ )	Value ( $m = 4$ )	Value ( $m = 6$ )	Value ( $m = 7.35$ )	Reference
$k_B$	J K <sup>-1</sup>	$1.38 \times 10^{-23}$	$1.38 \times 10^{-23}$	$1.38 \times 10^{-23}$	$1.38 \times 10^{-23}$	Commonly known
$v$	m <sup>3</sup>	$3 \times 10^{-29}$	$3 \times 10^{-29}$	$3 \times 10^{-29}$	$3 \times 10^{-29}$	Commonly known
$w_{PAA}$	–	0.032	0.0296	0.0276	0.0264	Theoretical value
$w_{PEG}$	–	0.968	0.9704	0.9724	0.9736	Theoretical value
$\rho_w$	g cm <sup>-3</sup>	1.0	1.0	1.0	1.0	Commonly known
$\rho_d$	g cm <sup>-3</sup>	1.09	1.09	1.09	1.09	Shah et al. (2006)
$T$	K	310	310	310	310	Diederich et al. (2017)
$G_0$	kPa	46	26	24	16.0	Diederich et al. (2017)
$J_m$	–	1000	1000	1000	1000	Fitted
$\chi_1$	–	0.6574	0.6561	0.6208	0.6521	Fitted
$\chi_2$	–	0.1754	0.1649	0.1212	0.1545	Fitted
$N$	–	25	25	25	25	Fitted
$k'$	day <sup>-1</sup>	$8.5 \times 10^{-3}$	$9.17 \times 10^{-3}$	$9.17 \times 10^{-3}$	$8.5 \times 10^{-3}$	Fitted

concentration of polymer is larger, and this also translates into a larger number of cross-links per kinetic chain  $N$ . In contrast to Tetra-PEG hydrogels, here mass loss starts as soon as degradation starts, increases almost linearly throughout most of the degradation process, and eventually rises sharply in the final stage. The swelling ratio also shows a sharp transition between the early and later stages of the degradation process.

We next turn to hydrogels considered by Diederich et al. (2017), which were prepared from 4000 –  $m$  macromonomers with identical concentration, 10wt%, but different numbers  $m$  of lactide units per PLA segments. We note that the initial ground shear modulus  $G_0$  reported by Diederich et al. depends on the number of lactide units  $m$ , and decreases as  $m$  increases, which might be imputed to the increasing molecular weight of the macromonomer with increasing number of degradable units (Diederich et al., 2017). Material parameters used in the model were obtained similarly as in the previous example, and are collected in Table 3. Since the same macromonomer concentration is used for all the samples,  $N$  is also set to the same values for all samples.

The model predictions and experimental results are presented in Fig. 14. Fig. 14(a) shows the evolution of the extent of reaction  $\zeta$  with time predicted by the fully-coupled model, along with the predictions of the first-order kinetic model using the average reaction constant. Degradation follows first-order reaction kinetics with rate constant almost independent on  $m$ . The swollen modulus, mass loss fraction and mass swelling ratio are shown in Figs. 14(b)–(d), respectively. Here, we show the mass swelling ratio  $M = m_i(t)/m_d(t)$ , where  $m_i(t)$  and  $m_d(t)$  denote the masses of hydrogel and dry network at time  $t$ , respectively, in order to use the raw experimental data in Diederich et al. (2017). The relation between  $M$  and  $Q$  is expressed as  $M = 1 + (Q - 1)\rho_w/\rho_d$ , where  $\rho_w$  and  $\rho_d$  represent the densities of water and dry network, respectively. Larger values of  $m$  result in faster mass loss and swelling, which is well captured by the model.

In summary, the comparison of the time evolution of modulus, mass loss and swelling ratios observed in experiments and predicted by the model demonstrate that the proposed model is robust and accurate in capturing the coupled reaction, degradation, and deformation behaviour of biodegradable hydrogels, using a very limited number of fitting parameters.

## 7. Examples of homogeneous swelling due to degradation under load

The previous two sections illustrated the model capability in free swelling conditions. In this section, additional examples are given to illustrate the model response under externally-applied stresses. Throughout this section, the material properties previously identified for the PLA-b-PEG-b-PLA gel Sample-1 are used, cf. Table 2.

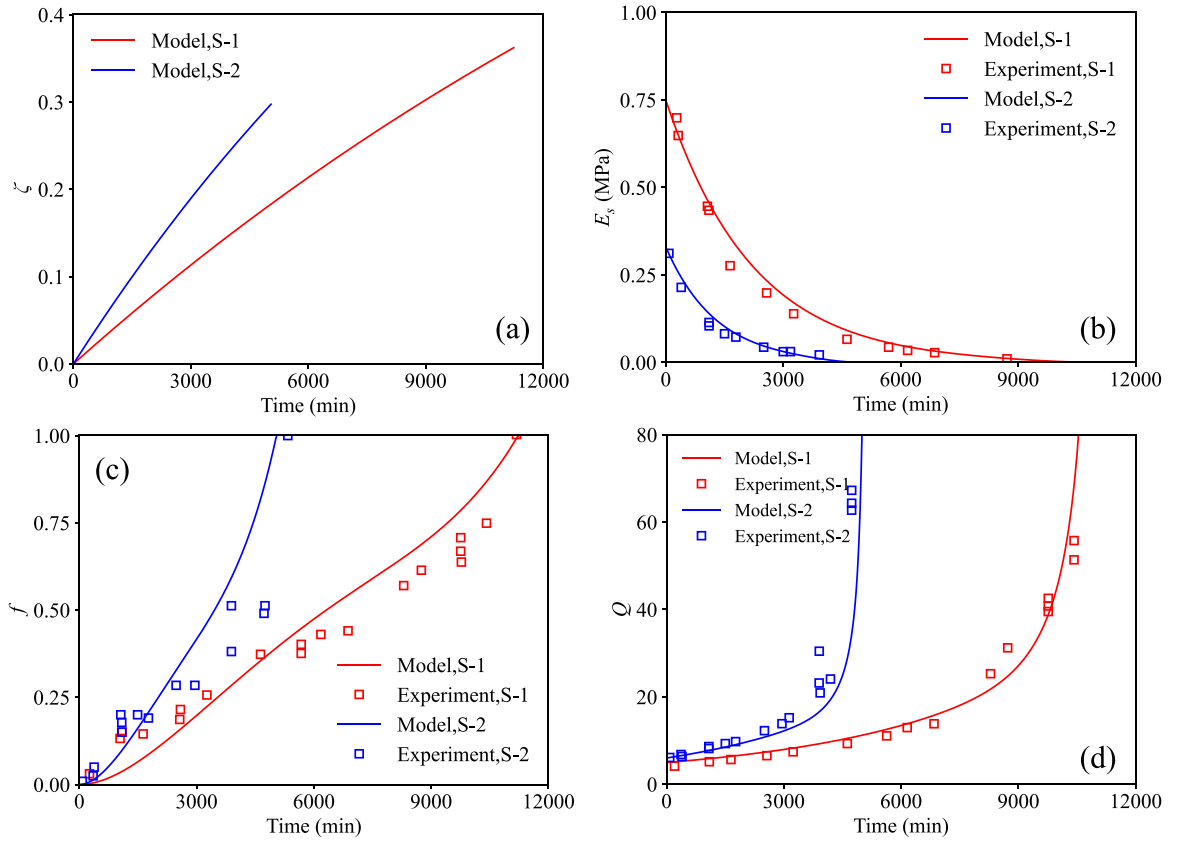


Fig. 13. Comparison of model predictions and experimental data reported by Metters et al. (2000a) for the free swelling of PLA-b-PEG-b-PLA hydrogels. Time evolution of (a) extent of reaction  $\zeta$ , (b) swollen modulus  $E_s$ , (c) mass loss fraction  $f$ , and (d) swelling ratio  $Q$ . The symbols denote the experimental data, while the lines represent the model predictions.

### 7.1. Stress relaxation

Consider a rectangular block of gel immersed in water and subjected to a prescribed stretch  $\lambda_1$ . Lateral surfaces are traction free. The prescribed stretch is held constant as the gel swells and degrades.

The principal elastic stretches are given by  $\lambda_1^e = \lambda_1/\lambda_s$  and  $(\lambda_2^e)^2 = (\lambda_3^e)^2 = 1/\lambda_1^e$ , where we used the condition of elastic incompressibility. Using the state law for the stress (28) together with the boundary conditions on the principal Cauchy stresses,  $\sigma_2 = \sigma_3 = 0$ , the hydrostatic pressure is identified:

$$\Pi = \frac{2}{\lambda_s} \frac{\partial \tilde{\psi}}{\partial \tilde{I}_1} \frac{\lambda_1^i}{\lambda_1} \quad (78)$$

The principal nominal stress in the direction of the applied stretch is then obtained using Eqs. (12), (39), and (78):

$$P_1 = \frac{2}{\lambda_s} \frac{\partial \tilde{\psi}}{\partial \tilde{I}_1} \left( \lambda_1 \lambda^i - \frac{\lambda_i^4}{\lambda_1^2} \right) \quad (79)$$

Inserting Eq. (78) into Eq. (42) and using the chemical equilibrium condition  $\mu = \mu_0$  leads to the following governing equation for the polymer fraction:

$$k_B T [\ln(1 - \phi) + \phi + (\chi_1 - \chi_2)\phi^2 + 2\chi_2\phi^3] + \frac{2}{\lambda_s} \frac{\partial \tilde{\psi}}{\partial \tilde{I}_1} \frac{\lambda_1^i}{\lambda_1} v = 0 \quad (80)$$

Given values of  $\lambda_1$  and  $\zeta$  at a given time, Eq. (80) is solved for the polymer fraction  $\phi$ . The stress (79) and driving force for chemical reaction (44) are calculated, and the extent of reaction is updated using the kinetic model (46) integrated using an explicit time-integration scheme, similar to the previous two sections.

Fig. 15 shows the swelling ratio  $Q(t) = \phi^{-1}(t)$  and nominal stress  $P_1(t)$  during degradation, for different values of the applied stretch  $\lambda_1$ . The stretch  $\lambda_1 = 1.7$  corresponds to the stretch of the undegraded material in free swelling conditions, identified from the results of the previous section. Therefore, at  $t = 0$ , the stress is zero for  $\lambda_1 = 1.7$ , while the gel is initially in compression for  $\lambda_1 = 0.8$  and  $\lambda_1 = 1$ , and in tension for  $\lambda_1 = 3$  and  $\lambda_1 = 5$ . Fig. 15(a) shows that the swelling ratio monotonically increases during

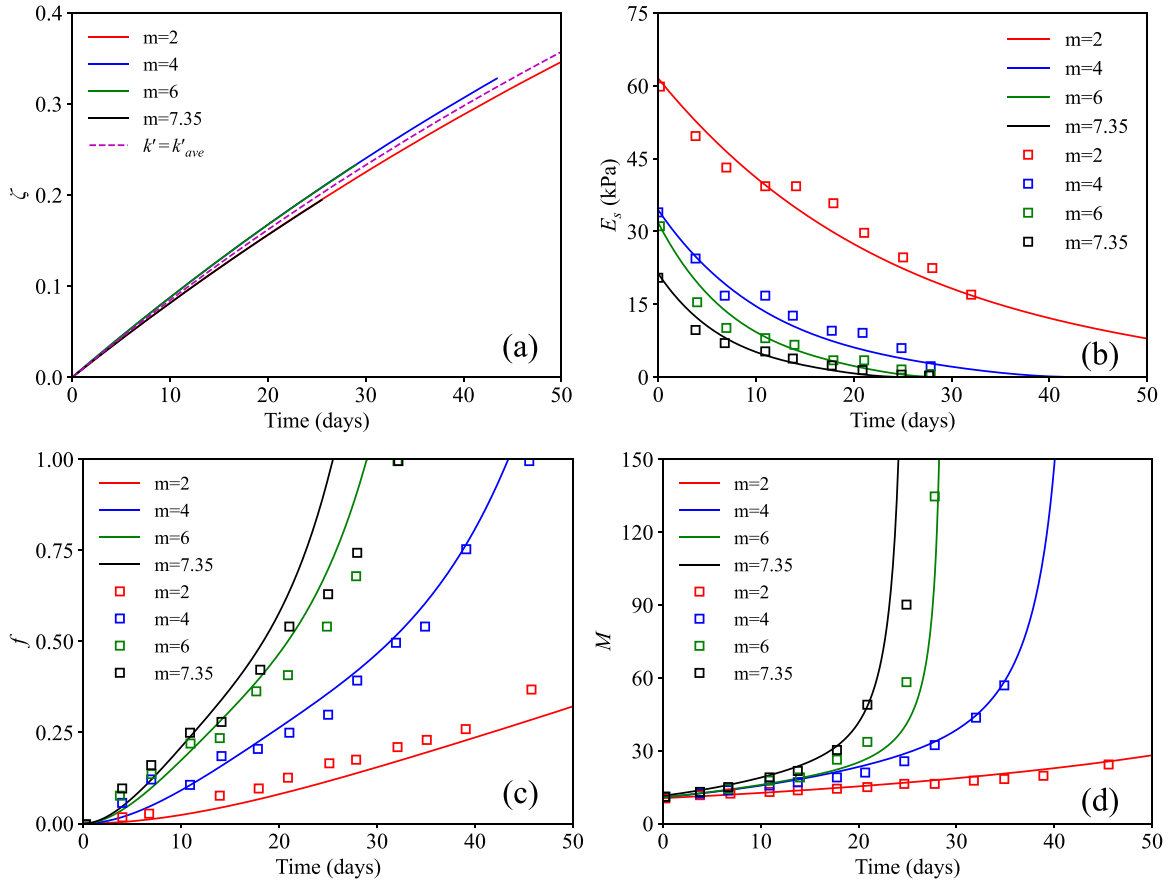


**Fig. 14.** Comparison of model predictions and experimental data reported by [Diederich et al. \(2017\)](#) for the free swelling of PLA-b-PEG-b-PLA hydrogels. Time evolution of (a) extent of reaction  $\zeta$ , (b) swollen modulus  $E_s$ , (c) mass loss fraction  $f$ , and (d) mass swelling ratio  $M$ . The symbols denote the experimental data, while the lines represent the model predictions.

degradation for all values of the applied stretch, as a result of the reduction in modulus. The effect of degradation on stress relaxation is more complex, as shown in [Fig. 15\(b\)](#), due to competing effect of swelling and modulus reduction. The competition between the two effects can be seen in the case where the hydrogel is initially stress free ( $\lambda_1 = 1.7$ ), see also the inset in the figure. At the early stages of degradation, a swelling-induced compressive stress is generated. However, degradation-induced modulus reduction quickly counterbalances this effect and the stress relaxes to zero as degradation progresses. When the hydrogel is initially under tension, both swelling and modulus reduction tend to decrease the stress. When the hydrogel is initially in compression, swelling and modulus reduction have opposite effects, but modulus reduction dominates and the stress monotonously decreases in magnitude.

## 7.2. Hydrostatic loading

Next consider a rectangular block of degradable gel subjected to prescribed hydrostatic (Cauchy) stress  $\bar{\sigma}$ . In this case, we have  $\lambda_i = \lambda^i$  and  $\lambda_i^e = 1$  ( $i = 1, 2, 3$ ). Using Eq. (39) with the boundary conditions  $\sigma_i = \bar{\sigma}$  ( $i = 1, 2, 3$ ), the hydrostatic pressure is obtained as

$$\Pi = \frac{2}{\lambda_s} \frac{\partial \bar{\psi}}{\partial \bar{I}_1} - \bar{\sigma} \quad (81)$$

Inserting this expression into Eq. (42) together with the condition  $\mu = \mu_0$  gives the following governing equation for the polymer volume fraction:

$$k_B T [\ln(1 - \phi) + \phi + (\chi_1 - \chi_2)\phi^2 + 2\chi_2\phi^3] + \left( \frac{2}{\lambda_s} \frac{\partial \bar{\psi}}{\partial \bar{I}_1} - \bar{\sigma} \right) v = 0 \quad (82)$$

from which the swelling ratio  $Q = \phi^{-1}$  can be obtained for given values of  $\bar{\sigma}$  and  $\zeta$ . The procedure to update  $\zeta$  is similar to the previous section.

The effect of  $\bar{\sigma}$  on  $Q(t)$  is shown in [Fig. 16](#). As compared to the free swelling case ( $\bar{\sigma} = 0$ ), a tensile hydrostatic stress increases the swelling ratio at a given time, as expected. In contrast, a compressive hydrostatic stress tends to squeeze water out of the hydrogel

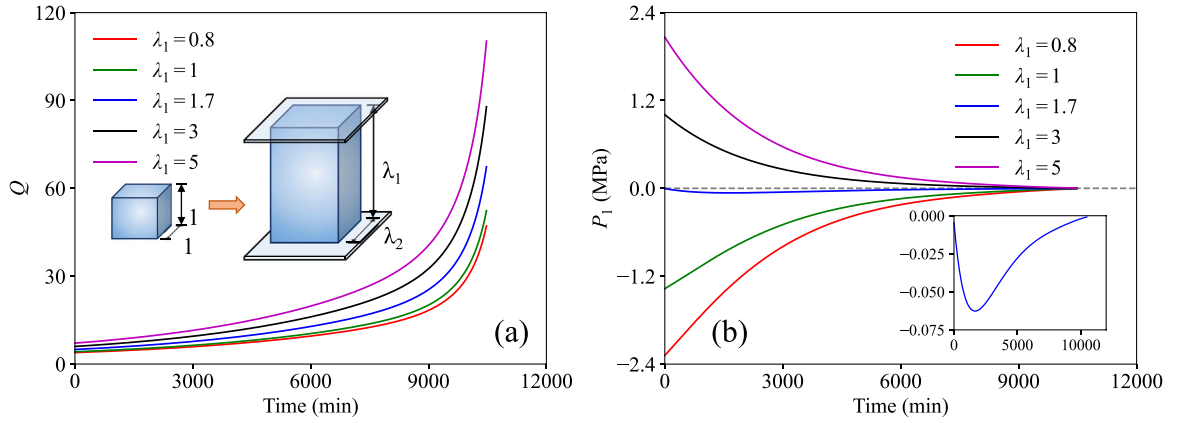


Fig. 15. A block of degradable hydrogel subjected to a fixed stretch  $\lambda_1$  in water. Time evolution of (a) the swelling ratio  $Q$  and (b) the uniaxial nominal stress  $P_1(t)$ .

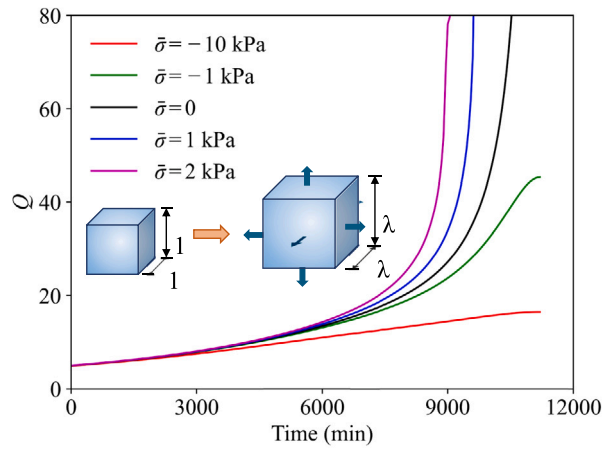


Fig. 16. Swelling ratio  $Q$  in a block of degradable hydrogel subjected to a constant hydrostatic stress  $\bar{\sigma}$ .

and leads to smaller swelling ratios up to the point of reverse gelation. Note that the point of reverse gelation ( $G = 0$ ) is reached at the same time in all cases. In other words, degradation kinetics is unaffected by stresses in this example, and first-order kinetics still prevails.

## 8. Heterogeneous swelling due to degradation

We have implemented our continuum framework and constitutive models for coupled deformation and degradation as user-subroutines for the finite element software ABAQUS. Specifically, the free energy function (32) together with its derivatives with respect to the strain invariants are defined in a user-defined subroutine for hyperelastic material (UHYPER). Updates for the degradation state  $\zeta$ , water concentration and mass loss  $f$  are calculated in a user-defined subroutine for a field variable (USDFLD). State variables updated in USDFLD are then passed to the UHYPER. Note that our implementation is completely general and accounts for the coupled contributions  $w_f$  and  $w_g$  to the degradation driving force. The hydrostatic pressure term  $\Pi$  in  $\omega_f$ , Eq. (45), was accessed using the function *GETVRM*, which can be called from the USDFLD subroutine but not from the UHYPER subroutine. Implementation of the fully coupled theory thus requires the combination of UHYPER and USDFLD. However, if one neglects the coupled terms  $w_f$  and  $w_g$  from the outset, the theory can be implemented as a UHYPER alone.

Numerical results reported below were obtained using the material properties of PLA-b-PEG-b-PLA gel, Sample-1, reported in Table 2. For these material properties the coupled contributions to the reaction driving force were found again to have negligible impact on the predictions. Therefore, our simulations only illustrate degradation-induced (heterogeneous) swelling resulting from modulus reduction and polymer mass loss, while deformation has negligible impact on degradation kinetics. We do not exclude however that two-way coupling could be significant in other hydrogel systems, and this can be handled by our general implementation.

### 8.1. Shape adaptation due to degradation-induced swelling

We first investigate degradation-induced swelling of a piece of hydrogel in a cavity with rigid walls. Shape adaptation during swelling is of significance in tissue engineering, for example for the treatment of bone defects with an irregular shape. Two scenarios are considered, namely: (1) the filling of a cuboid cavity with an initially cylindrical piece of gel and (2) the filling a cylindrical cavity with an initially cuboid piece of gel. Considering the symmetry of the problem, one quarter of the gel geometry is meshed for efficiency. The hydrogels in scenarios (1) and (2) are discretised using 320 and 400 C3D8 elements, respectively. The container is modelled using the analytical rigid body, and hard contact is applied between the gel and the container.

In the simulations, a block of the dry network is put into the cavity and let to swell (instantaneously) to equilibrium. The fully-swollen, undegraded gel is smaller than the cavity, so that initial swelling is homogeneous and stress free. Then, axial displacement constraints are applied on both the top and bottom faces of the hydrogel while traction free conditions are set in the lateral direction. As degradation proceeds, the hydrogel swells further and fills the cavity. Cross-sectional contour plots of the nominal swelling ratio  $J$  at different degradation times for the two scenarios are presented in Figs. 17 and 18, respectively. The hydrogel can adapt well to the cavity shape. A higher compressive stress is generated in the contact region, leading to a smaller nominal swelling ratio since a compressive stress hinders the absorption of water.

### 8.2. Degradation of a porous cubic representative volume cell

We next consider degradation-induced swelling of a porous lattice scaffold, which is relevant for tissue engineering applications. A representative unit cell (UC) of the porous lattice is shown in Fig. 19(a). The geometry of the UC is characterised by the ratio  $e/l$ , where  $e$  is the pillar thickness and  $l$  is the cell edge. The UCs are discretised using 4000 C3D8 elements. We first let the gel swell to equilibrium under free conditions by applying zero normal displacement condition on the three outer surfaces that are adjacent to each other. Then, zero normal displacement boundary conditions are applied on all the six outer faces, and traction free conditions are set on the other faces. To avoid interpenetration between the adjacent edges, self-contact interaction is specified for the whole model.

The contour plots of nominal swelling ratio  $J$  in the UCs with  $e/l = 0.15, 0.2$  and  $0.25$  after 10000 min of degradation are presented in Figs. 19(b), (c), and (d), respectively. Regions near to the vertexes and corners are subjected to a higher compressive stress, which leads to a smaller swelling ratio, while regions near the edge interior have a larger swelling ratio due to free condition. Fig. 20 shows the time evolution of the reaction force generated on each of the surrounding walls of the UC. The combined effect of modulus reduction and swelling of the UC results in an increase first, and a decrease afterward, in the absolute value of the reaction force. All the curves reach the peak after around 2000 min of degradation.

## 9. Conclusions

We have proposed a general thermodynamically consistent framework for biodegradable hydrogels coupling hydrolytic degradation and large deformations under the assumption of fast diffusion of mobile species (water and short chains), and negligible concentration of the short chains. The fast diffusion assumption holds given the long degradation time scale, over which diffusion phenomena are in a pseudo steady state with respect to degradation. Evolution equations for degradation were formulated, accounting for coupled contributions to the degradation driving force arising from concurrent elastic deformation and swelling. We further proposed specific constitutive models for model degradable hydrogels previously investigated in the literature. In particular, physically-based models were proposed for the elastic modulus and mass loss fraction, which account for the particular network topology and degradation mechanisms. We have compared the predictions of our model with available experimental data for degradable hydrogels in free swelling conditions. Model parameters were taken directly from the experiments whenever possible, so that the number of fitting parameters was kept to a minimum. The model was shown to reproduce experimental observations very well. In the considered examples, we found that coupled effects in the reaction driving force are negligible, and that the extent of reaction essentially follows a first-order kinetics. We have also considered several computational case studies that mimic possible scenarios relevant to biomedical applications. These studies highlighted the role of external constraints on degradation-induced, inhomogeneous swelling.

As future work, the thermodynamic framework could be generalised to account for non-negligible concentration of reaction products within the gels. This would require a generalisation of the free energy imbalance (14) to include the chemical power supplied by all species involved, along with their conservation equations linked by reaction stoichiometry. Such generalisation would enable us to describe the effect of reaction products on the osmotic pressure and reaction kinetics, see e.g. Zhou and Jin (2020). Other generalisation could include a description of drug/cell release in biodegradable hydrogel-based delivery systems, as well as a description of other degradation mechanisms (e.g. enzymatic degradation).

### CRediT authorship contribution statement

**Zhouzhou Pan:** Methodology, Software, Investigation, Validation, Writing – original draft. **Laurence Brassart:** Conceptualization, Methodology, Supervision, Funding acquisition, Writing – review & editing.



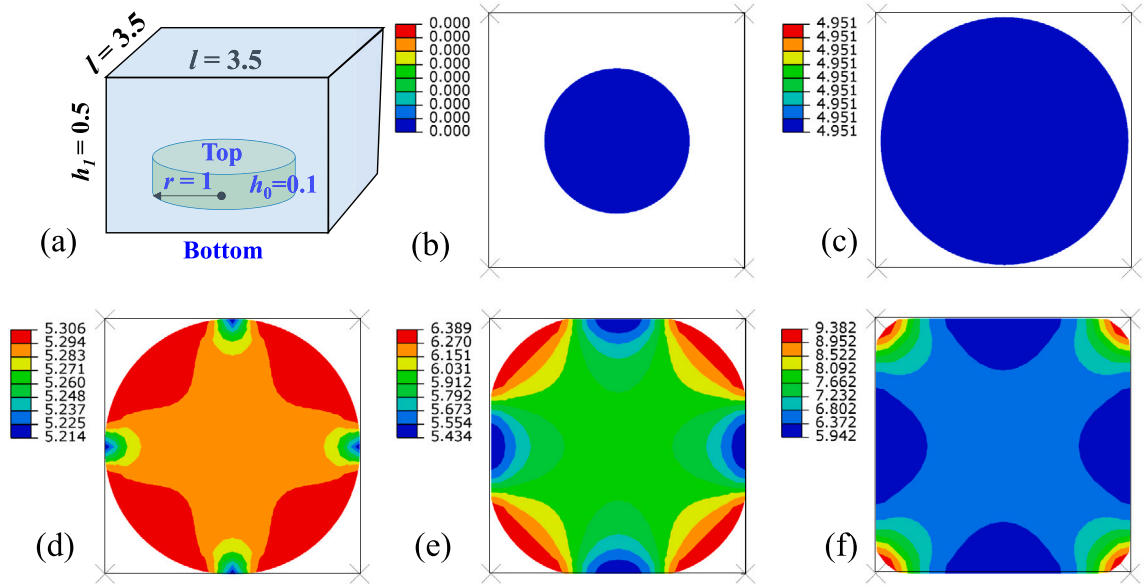


Fig. 17. (a) Schematic of a cylindrical gel filling a cuboid cavity. Cross-sectional contour plots of nominal swelling ratio  $J$  in (b) the dry state, (c) the initial freely-swollen state, and after (d) 750 min, (e) 2100 min, and (f) 10950 min of degradation.

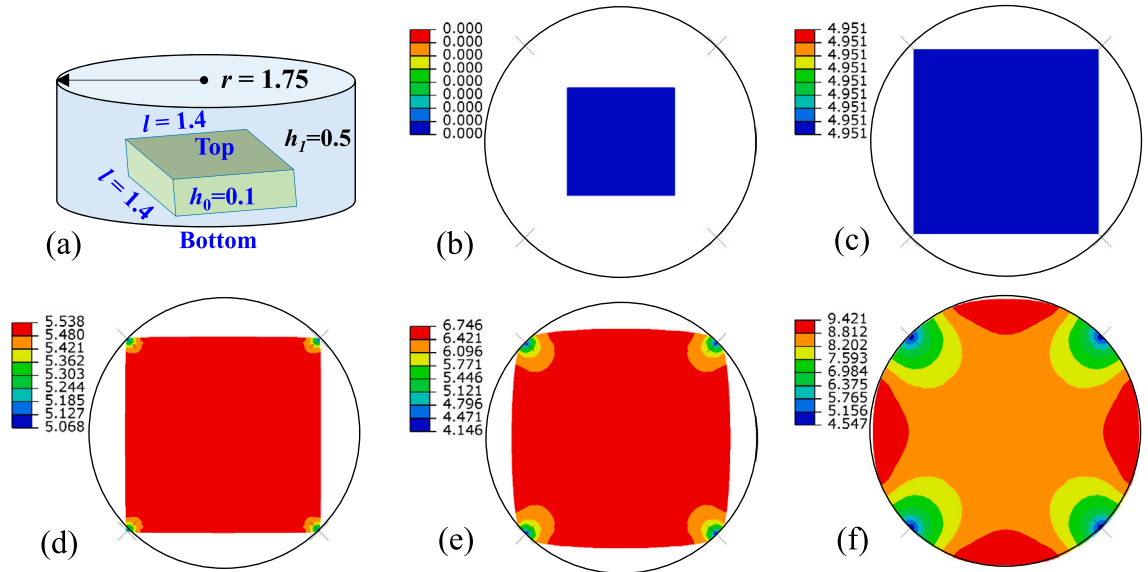


Fig. 18. (a) Schematic of a cuboid gel filling a cylindrical cavity. Cross-sectional contour plots of nominal swelling ratio  $J$  in (b) the dry state, (c) the initial freely-swollen state, and after (d) 1200 min, (e) 6800 min, and (f) 11000 min of degradation.

### Declaration of competing interest

The authors declare that they have no known competing financial interests or personal relationships that could have appeared to influence the work reported in this paper.

### Data availability

Data will be made available on request.

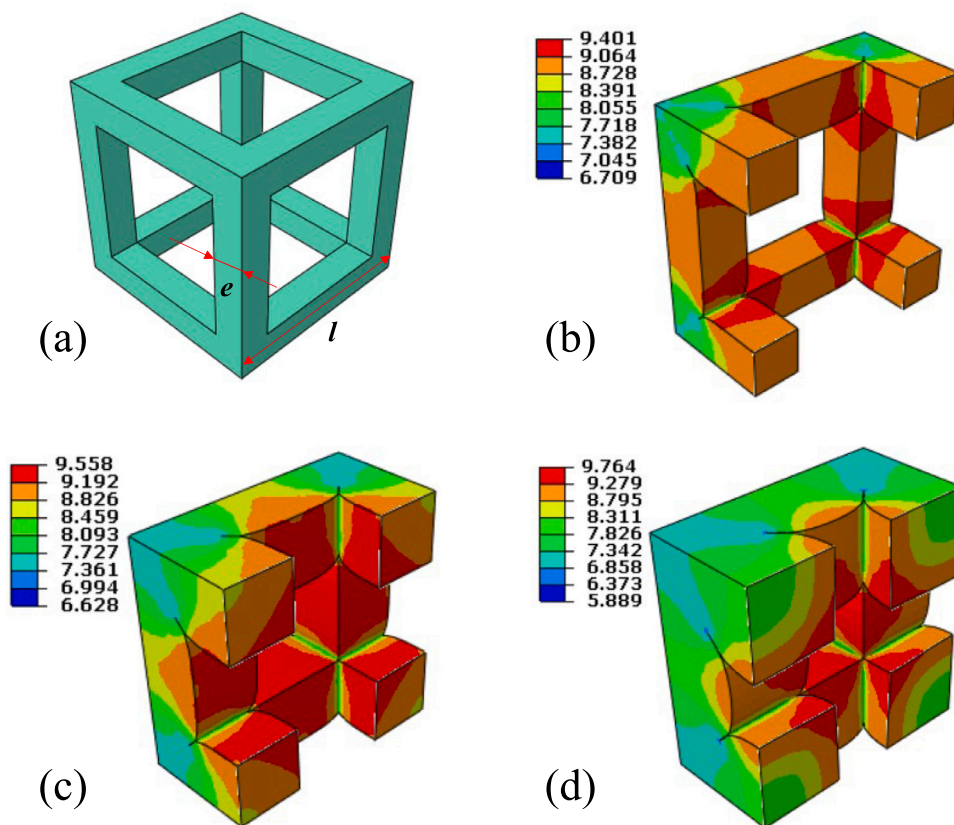


Fig. 19. (a) Unit cell of a porous cubic scaffold. Contour plots of nominal swelling ratio  $J$  in the degrading scaffold with (b)  $e/l = 0.15$ , (c)  $e/l = 0.2$ , and (d)  $e/l = 0.25$  after 10000 min of degradation. Only half of the cell is presented for clarity.

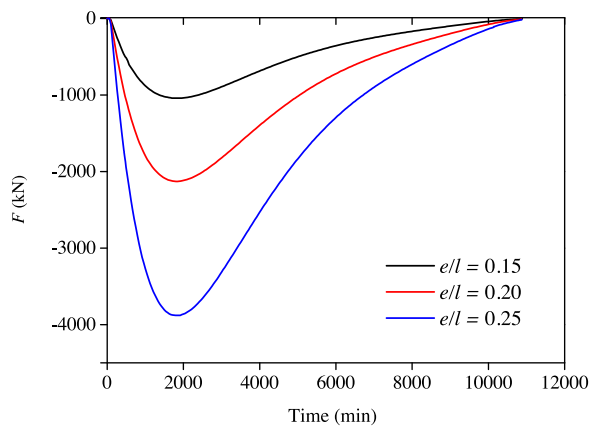


Fig. 20. Time evolution of the reaction force generated on each of the surrounding walls of the UC.

## Acknowledgement

This work was supported by a New Investigator Award of the Engineering and Physical Sciences Research Council [EP/V032755/1].

## References

- Akagi, Y., Gong, J., Chung, U.i., Sakai, T., 2013. Transition between phantom and affine network model observed in polymer gels with controlled network structure. *Macromolecules* 46, 1035–1040. <http://dx.doi.org/10.1021/ma302270a>.

- Alamé, G., Brassart, L., 2019. Relative contributions of chain density and topology to the elasticity of two-dimensional polymer networks. *Soft Matter* 15 (28), 5703–5713. <http://dx.doi.org/10.1039/C9SM00796B>.
- Alamé, G., Brassart, L., 2020. Effect of topological defects on the elasticity of near-ideal polymer networks. *J. Appl. Mech.* 87 (12), <http://dx.doi.org/10.1115/1.4048316>.
- Amsden, B., 1998. Solute diffusion within hydrogels. Mechanisms and models. *Macromolecules* 31 (23), 8382–8395. <http://dx.doi.org/10.1021/ma980765f>.
- Bahrololoumi, A., Mohammadi, H., Moravati, V., Dargazany, R., 2021a. A physically-based model for thermo-oxidative and hydrolytic aging of elastomers. *Int. J. Mech. Sci.* 194, <http://dx.doi.org/10.1016/j.ijmecsci.2020.106193>.
- Bahrololoumi, A., Morovati, V., Poshtan, E.A., Dargazany, R., 2020. A multi-physics constitutive model to predict hydrolytic aging in quasi-static behaviour of thin cross-linked polymers. *Int. J. Plast.* 130, <http://dx.doi.org/10.1016/j.ijplas.2020.102676>.
- Bahrololoumi, A., Morovati, V., Shaafe, M., Dargazany, R., 2021b. A multi-physics approach on modeling of hygrothermal aging and its effects on constitutive behavior of cross-linked polymers. *J. Mech. Phys. Solids* 156, <http://dx.doi.org/10.1016/j.jmps.2021.104614>.
- Bosnjak, N., Nadimpalli, S., Okumura, D., Chester, S., 2020. Experiments and modeling of the viscoelastic behavior of polymeric gels. *J. Mech. Phys. Solids* 137, 103829. <http://dx.doi.org/10.1016/j.jmps.2019.103829>.
- Bryant, S., Vernerey, F., 2018. Programmable hydrogels for cell encapsulation and neo-tissue growth to enable personalized tissue engineering. *Adv. Healthc. Mater.* 7, 1700605. <http://dx.doi.org/10.1002/adhm.201700605>.
- Castilla-Cortázar, I., Más-Estellés, J., Meseguer-Dueñas, J.M., Ivirico, J.E., Marí, B., Vidaurre, A., 2012. Hydrolytic and enzymatic degradation of a poly ( $\epsilon$ -caprolactone) network. *Polym. Degrad. Stab.* 97 (8), 1241–1248. <http://dx.doi.org/10.1016/j.polymdegradstab.2012.05.038>.
- Cha, C., Kohman, R.H., Kong, H., 2009. Biodegradable polymer crosslinker: independent control of stiffness, toughness, and hydrogel degradation rate. *Adv. Funct. Mater.* 19 (19), 3056–3062. <http://dx.doi.org/10.1002/adfm.200900865>.
- Chester, S.A., Anand, L., 2010. A coupled theory of fluid permeation and large deformations for elastomeric materials. *J. Mech. Phys. Solids* 58 (11), 1879–1906. <http://dx.doi.org/10.1016/j.jmps.2010.07.020>.
- Dhote, V., Vernerey, F.J., 2014. Mathematical model of the role of degradation on matrix development in hydrogel scaffold. *Biomech. Model. Mechanobiol.* 13 (1), 167–183. <http://dx.doi.org/10.1007/s10237-013-0493-0>.
- Diederich, V.E.G., Villiger, T., Storti, G., Lattuada, M., 2017. Modeling of the degradation of poly(ethylene glycol)-co-(lactic acid)-dimethacrylate hydrogels. *Macromolecules* 50 (14), 5527–5538. <http://dx.doi.org/10.1021/acs.macromol.7b00902>.
- Drozdov, A., 2017. Modeling the response of double-network gels with sacrificial junctions under swelling. *Int. J. Solids Struct.* 122–123, 175–188. <http://dx.doi.org/10.1016/j.ijsolstr.2017.06.013>.
- Flory, P.J., 1942. Thermodynamics of high polymer solutions. *J. Chem. Phys.* 10 (1), 51–61. <http://dx.doi.org/10.1063/1.1723621>.
- Flory, P., 1976. Statistical thermodynamics of random networks. *Proc. R. Soc. Lond.* 351, 351–380. <http://dx.doi.org/10.1098/rspa.1976.0146>.
- Flory, P.J., Rehner, J., 1943. Statistical mechanics of cross-linked polymer networks I. Rubberlike elasticity. *J. Chem. Phys.* 11 (11), 512–520. <http://dx.doi.org/10.1063/1.1723791>.
- Fu, X., Hosta-Rigau, L., Chandrawati, R., Cui, J., 2018. Multi-stimuli-responsive polymer particles, films, and hydrogels for drug delivery. *Chem* 4, 2084–2107. <http://dx.doi.org/10.1016/j.chempr.2018.07.002>.
- Fujiiyabu, T., Li, X., Chung, U.I., Sakai, T., 2019. Diffusion behavior of water molecules in hydrogels with controlled network structure. *Macromolecules* 52 (5), 1923–1929. <http://dx.doi.org/10.1021/acs.macromol.8b02488>.
- Gent, A.N., 1996. A new constitutive relation for rubber. *Rubber Chem. Technol.* 69 (1), 59–61. <http://dx.doi.org/10.5254/1.3538357>.
- Gilormini, P., Richaud, E., Verdu, J., 2014. A statistical theory of polymer network degradation. *Polymer* 55, 3811–3817. <http://dx.doi.org/10.1016/j.polymer.2014.05.008>.
- Graessley, W., 1975. Statistical mechanics of random coil networks. *Macromolecules* 8 (2), 186–190. <http://dx.doi.org/10.1021/ma60044a017>.
- Hajikhani, A., Wriggers, P., Marino, M., 2021. Chemo-mechanical modelling of swelling and crosslinking reaction kinetics in alginate hydrogels: A novel theory and its numerical implementation. *J. Mech. Phys. Solids* 153, <http://dx.doi.org/10.1016/j.jmps.2021.104476>.
- Hong, W., Zhao, X., Zhou, J., Suo, Z., 2008. A theory of coupled diffusion and large deformation in polymeric gels. *J. Mech. Phys. Solids* 56 (5), 1779–1793. <http://dx.doi.org/10.1016/j.jmps.2007.11.010>.
- Huang, R., Zheng, S., Liu, Z., Ng, T.Y., 2020. Recent advances of the constitutive models of smart materials - hydrogels and shape memory polymers. *Int. J. Appl. Mech.* 12 (02), <http://dx.doi.org/10.1142/s1758825120500143>.
- Huggins, M.L., 1942. Some properties of solutions of long-chain compounds. *J. Phys. Chem.* 46 (1), 151–158. <http://dx.doi.org/10.1021/j150415a018>.
- Kamata, H., Li, X., Chung, U.I., Sakai, T., 2015. Design of hydrogels for biomedical applications. *Adv. Healthc. Mater.* 4, 2360–2374. <http://dx.doi.org/10.1002/adhm.201500076>.
- Konica, S., Sain, T., 2020. A thermodynamically consistent chemo-mechanically coupled large deformation model for polymer oxidation. *J. Mech. Phys. Solids* 137, 103858. <http://dx.doi.org/10.1016/j.jmps.2019.103858>.
- Konica, S., Sain, T., 2021. A homogenized large deformation constitutive model for high temperature oxidation in fiber-reinforced polymer composites. *Mech. Mater.* 160, <http://dx.doi.org/10.1016/j.mechmat.2021.103994>.
- Kothari, K., Hu, Y., Gupta, S., Elbanna, A., 2018. Mechanical response of two-dimensional polymer networks: role of topology, rate dependence, and damage accumulation. *J. Appl. Mech.* 85 (3), <http://dx.doi.org/10.1115/1.4038883>.
- Lamont, S., Mulderrig, J., Bouklas, N., Vernerey, F., 2021. Rate-dependent damage mechanics of polymer networks with reversible bonds. *Macromolecules* 54, 10801–10813. <http://dx.doi.org/10.1021/acs.macromol.1c01943>.
- Lei, J., Li, Z., Xu, S., Liu, Z., 2021a. A mesoscopic network mechanics method to reproduce the large deformation and fracture process of cross-linked elastomers. *J. Mech. Phys. Solids* 156, 104599. <http://dx.doi.org/10.1016/j.jmps.2021.104599>.
- Lei, J., Li, Z., Xu, S., Liu, Z., 2021b. Recent advances of hydrogel network models for studies on mechanical behaviors. *Acta Mech. Sin.* 37, 367–386. <http://dx.doi.org/10.1007/s10409-021-01058-2>.
- Li, J., Mooney, D.J., 2016. Designing hydrogels for controlled drug delivery. *Nature Rev. Mater.* 1 (12), <http://dx.doi.org/10.1038/natrevmats.2016.71>.
- Li, X., Tsutsui, Y., Matsunaga, T., Shibayama, M., Chung, U.I., Sakai, T., 2011. Precise control and prediction of hydrogel degradation behavior. *Macromolecules* 44, 3567–3571. <http://dx.doi.org/10.1021/ma2004234>.
- Liu, D., Ma, S., Yuan, H., Markert, B., 2022. Computational modelling of poro-visco-hyperelastic effects on time-dependent fatigue crack growth of hydrogels. *Int. J. Plast.* 155, 103307. <http://dx.doi.org/10.1016/j.ijplas.2022.103307>.
- Liu, Z., Toh, W., Ng, T.Y., 2015. Advances in mechanics of soft materials: A review of large deformation behavior of hydrogels. *Int. J. Appl. Mech.* 7 (05), 1530001. <http://dx.doi.org/10.1142/S1758825115300011>.
- Loeffel, K., Anand, L., 2011. A chemo-thermo-mechanically coupled theory for elastic-viscoplastic deformation, diffusion, and volumetric swelling due to a chemical reaction. *Int. J. Plast.* 27 (9), 1409–1431. <http://dx.doi.org/10.1016/j.ijplas.2011.04.001>.
- Lu, T., Wang, Z., Tang, J., Zhang, W., Wang, T., 2020. A pseudo-elasticity theory to model the strain-softening behavior of tough hydrogels. *J. Mech. Phys. Solids* 137, 103832. <http://dx.doi.org/10.1016/j.jmps.2019.103832>.
- Lucantonio, A., Nardinocchi, P., Teresi, L., 2013. Transient analysis of swelling-induced large deformations in polymer gels. *J. Mech. Phys. Solids* 61 (1), 205–218. <http://dx.doi.org/10.1016/j.jmps.2012.07.010>.
- Lueckgen, A., Garske, D.S., Ellinghaus, A., Desai, R.M., Stafford, A.G., Mooney, D.J., Duda, G.N., Cipitria, A., 2018. Hydrolytically-degradable click-crosslinked alginate hydrogels. *Biomaterials* 181, 189–198. <http://dx.doi.org/10.1016/j.biomaterials.2018.07.031>.

- Mao, Y., Lin, S., Zhao, X., Anand, L., 2017. A large deformation viscoelastic model for double-network hydrogels. *J. Mech. Phys. Solids* 100, 103–130. <http://dx.doi.org/10.1016/j.jmps.2016.12.011>.
- Mark, J., Erman, B., 2007. *Rubberlike Elasticity: A Molecular Primer*, second ed. Cambridge University Press.
- Metters, A.T., Anseth, K.S., Bowman, C.N., 2000a. Fundamental studies of a novel, biodegradable PEG-b-PLA hydrogel. *Polymer* 41 (11), 3993–4004. [http://dx.doi.org/10.1016/S0032-3861\(99\)00629-1](http://dx.doi.org/10.1016/S0032-3861(99)00629-1).
- Metters, A.T., Anseth, K.S., Bowman, C.N., 2001b. A statistical kinetic model for the bulk degradation of PLA-b-PEG-b-PLA hydrogel networks: incorporating network non-idealities. *J. Phys. Chem. B* 105 (34), 8069–8076. <http://dx.doi.org/10.1021/jp004083h>.
- Metters, A.T., Bowman, C.N., Anseth, K.S., 2000b. A statistical kinetic model for the bulk degradation of PLA-b-PEG-b-PLA hydrogel networks. *J. Phys. Chem. B* 104 (30), 7043–7049. <http://dx.doi.org/10.1021/jp000523t>.
- Metters, A., Bowman, C., Anseth, K., 2001a. Verification of scaling laws for degrading PLA-b-PEG-b-PLA hydrogels. *AIChE J.* 47 (6), 1432–1437. <http://dx.doi.org/10.1002/aic.690470619>.
- Miller, D., Macosko, C., 1976. A new derivation of post gel properties of network polymers. *Macromolecules* 9, 206–211. <http://dx.doi.org/10.5254/1.3535009>.
- Morovati, V., Dargazany, R., 2019. Micro-mechanical modeling of the stress softening in double-network hydrogels. *Int. J. Solids Struct.* 164, 1–11. <http://dx.doi.org/10.1016/j.ijsolstr.2019.01.002>.
- Najmeddine, A., Xu, Z., Liu, G., Croft, Z.L., Liu, G.G., Esker, A.R., Shakiba, M., 2022. Physics and chemistry-based constitutive modeling of photo-oxidative aging in semi-crystalline polymers. *Int. J. Solids Struct.* 111427. <http://dx.doi.org/10.1016/j.ijsolstr.2022.111427>.
- Nishi, K., Chijiishi, M., Katsumoto, Y., Nakao, T., Fujii, K., Chung, U.I., Noguchi, H., Sakai, T., Shibayama, M., 2012. Rubber elasticity for incomplete polymer networks. *J. Chem. Phys.* 137 (22), 224903. <http://dx.doi.org/10.1063/1.4769829>.
- Nishi, K., Fujii, K., Chung, U.I., Shibayama, M., Sakai, T., 2017. Experimental observation of two features unexpected from the classical theories of rubber elasticity. *Phys. Rev. Lett.* 119 (26), 267801. <http://dx.doi.org/10.1103/PhysRevLett.119.267801>.
- Pan, J., 2014. *Modelling Degradation of Bioresorbable Polymeric Medical Devices*. Elsevier.
- Park, H., Park, K., Shalaby, W.S., 1993. *Biodegradable Hydrogels for Drug Delivery*. CRC Press.
- Rizzo, F., Kehr, N., 2021. Recent advances in injectable hydrogels for controlled and local drug delivery. *Adv. Healthc. Mater.* 10, 2001341. <http://dx.doi.org/10.1002/adhm.202001341>.
- Rubinstein, M., Colby, R.H., 2003. *Polymer Physics*. Oxford University Press.
- Sakai, T., Matsunaga, T., Yamamoto, Y., Ito, C., Yoshida, R., Suzuki, S., Sasaki, N., Shibayama, M., Chung, U.I., 2008. Design and fabrication of a high-strength hydrogel with ideally homogeneous network structure from tetrahedron-like macromonomers. *Macromolecules* 41, 5379–5384. <http://dx.doi.org/10.1021/ma800476x>.
- Sakumichi, N., Yoshikawa, Y., Sakai, T., 2021. Linear elasticity of polymer gels in terms of negative energy elasticity. *Polym. J.* 53, 1293–1303. <http://dx.doi.org/10.1038/s41428-021-00529-4>.
- Shah, N.M., Pool, M.D., Metters, A.T., 2006. Influence of network structure on the degradation of photo-cross-linked PLA-b-PEG-b-PLA hydrogels. *Biomacromolecules* 7 (11), 3171–3177. <http://dx.doi.org/10.1021/bm060339z>.
- Shi, J., Yu, L., Ding, J., 2021. PEG-based thermosensitive and biodegradable hydrogels. *Acta Biomater.* 128, 42–59. <http://dx.doi.org/10.1016/j.actbio.2021.04.009>.
- Slaughter, B.V., Khurshid, S.S., Fisher, O.Z., Khademhosseini, A., Peppas, N.A., 2009. Hydrogels in regenerative medicine. *Adv. Mater.* 21 (32–33), 3307–3329. <http://dx.doi.org/10.1002/adma.200802106>.
- Stauffer, D., Aharony, A., 1994. *Introduction to Percolation Theory: Revised Second Edition*. Taylor & Francis.
- Ulm, F.J., Coussy, O., Kefei, L., Larive, C., 2000. Thermo-chemo-mechanics of ASR expansion in concrete structures. *J. Eng. Mech.* 126 (3), 233–242. [http://dx.doi.org/10.1061/\(asce\)0733-9399\(2000\)126:3\(233\)](http://dx.doi.org/10.1061/(asce)0733-9399(2000)126:3(233)).
- Wagner, R., Dai, J., Su, X., Vernerey, F., 2022. A mesoscale model for the micromechanical study of gels. *J. Mech. Phys. Solids* 167, 104982. <http://dx.doi.org/10.1016/j.jmps.2022.104982>.
- Wang, Q., Gao, Z., Yu, K., 2017. Interfacial self-healing of nanocomposite hydrogels: Theory and experiment. *J. Mech. Phys. Solids* 109, 288–306. <http://dx.doi.org/10.1016/j.jmps.2017.08.004>.
- Wang, D.K., Varanasi, S., Hill, D.J., Rasoul, F., Symons, A.L., Whittaker, A.K., 2012. The influence of composition on the physical properties of PLA-PEG-PLA-co-Boltorn based polyester hydrogels and their biological performance. *J. Mater. Chem.* 22 (14), 6994–7004. <http://dx.doi.org/10.1039/C2JM00039C>.
- Xue, X., Hu, Y., Deng, Y., Su, J., 2021. Recent advances in design of functional biocompatible hydrogels for bone tissue engineering. *Adv. Funct. Mater.* 31, 2009432. <http://dx.doi.org/10.1002/adfm.202009432>.
- Yoshikawa, Y., Sakumichi, N., Chung, U.I., Sakai, T., 2021. Negative energy elasticity in a rubberlike gel. *Phys. Rev. X* 11, 011045. <http://dx.doi.org/10.1103/PhysRevX.11.011045>.
- Zhou, Y., Jin, L., 2020. Hydrolysis-induced large swelling of polyacrylamide hydrogels. *Soft Matter* 16 (24), 5740–5749. <http://dx.doi.org/10.1039/d0sm00663g>.
- Zhou, Z., Lei, J., Liu, Z., 2022. Effect of water content on physical adhesion of polyacrylamide hydrogels. *Polymer* 246, 124730. <http://dx.doi.org/10.1016/j.polymer.2022.124730>.
- Zustiak, S.P., Leach, J.B., 2010. Hydrolytically degradable poly (ethylene glycol) hydrogel scaffolds with tunable degradation and mechanical properties. *Biomacromolecules* 11 (5), 1348–1357. <http://dx.doi.org/10.1021/bm100137q>.